Modelling and elucidation of the kinetics of multiple consecutive photoreactions $AB_4(4\Phi)$ with Φ-order kinetics. Application to the photodegradation of riboflavin.

Mounir Maafi*, Wassila Maafi

Leicester School of Pharmacy, De Montfort University, The Gateway, Leicester LE1 9BH, UK

* Corresponding author.

Tel.: +44 116 257 7704;

Fax: +44 116 257 7287.

E-mail address: mmaafi@dmu.ac.uk (M. Maafi)

Abstract

New semi-empirical rate-law system of equations is proposed for the first time for consecutive photoreactions that involving up to four photoreaction steps, $AB_4(4\Phi)$. The equation system was developed, tested and validated against synthetic kinetic traces generated by fifth-order Runge-Kutta (RK-5) calculations. The model accurately fitted the kinetic traces of Riboflavin photodegradation in ethanol which decomposes via the $AB_2(2\Phi)$ mechanism involving two consecutive photoreaction steps. A kinetic elucidation methodology useful for consecutive photoreactions was also proposed to determine all the kinetic parameters and reaction attributes defining $AB_2(2\Phi)$ reactions. The quantum yields of photodegradation, determined for wavelengths in the visible region 400-480 nm, ranged from 0.005 to 0.00756 and 0.0012 to 8 10^{-5} for the first and second photoreaction steps, respectively. They were found to increase with wavelength in defined sigmoid functions. For this monochromatic irradiation range, Riboflavin proved to be a useful actinometer. Finally, a photodegradation scale based on *pseudo*-rate-constant values was also proposed for drugs. This scale (including four groups) is thought to contribute to rationalizing photodegradation testing and might prove useful in categorizing drugs' photodegradation reactivity.

Keywords: Riboflavin, photodegradation, consecutive photoreactions, Φ-order photokinetics, actinometry, quantum yields, pseudo-rate-constant.

1. Introduction

Photokinetics of consecutive reactions are ubiquitous in both photochemical and pharmaceutical systems.[1-5] However, their kinetic description has remained unresolved in the literature where only the classical mathematical treatments are proposed for such purposes.[6-8] These treatments, originally developed for reactions governed by purely thermal processes, do not take into account the specificities relative to the interaction of the reacting species with light. Conceptually, the differential equations characterising photoreactions in general and drugs' photodegradation in particular have a different formulation to those established for thermal reactions. A difference that implies that the integrated rate-laws of phototransformations should not mathematically be equivalent to those derived for 0^{th}-, 1^{st}- and 2^{nd}-order reactions, for example. Indeed, photoreactions have been proven to obey Φ-order kinetics that typically involves a logarithmic function embedding an exponential term (the log-exp function) for the description of the variation of the reacting species concentrations' with time (the integrated rate-laws).[9,10] As a closed-form integration of the systems of differential equations relative to photoreactions is not generally possible,[11] a method was devised to derive validated semi-empirical integrated rate-laws for such reaction systems.[12,13] This approach was applied here, for the first time, to $AB_4(4\Phi)$ reactions involving four consecutive reaction-steps (each defined by a unique quantum yield Φ) where an initial species (A) sequentially leads to four photoproducts (B_{1-4}) , as depicted in Scheme 1.

$$\mathbf{A} \xrightarrow{\Phi_{A\rightarrow B1}} \mathbf{B_1} \xrightarrow{\Phi_{B1\rightarrow B2}} \mathbf{B_2} \xrightarrow{\Phi_{B2\rightarrow B3}} \mathbf{B_3} \xrightarrow{\Phi_{B3\rightarrow B4}} \mathbf{B_4}$$

Scheme 1: The reaction mechanism for $AB_4(4\Phi)$ consecutive photoreactions.

68 The developed semi-empirical equations were used here to investigate the
69 photodegradation kinetics of Riboflavin (Ribo), as an illustration example. Ribo, also known
70 as vitamin B_2 is a water soluble vitamin that is widely consumed.[14,15] It is present in various
71 food products such as liver, kidney, eggs, meat, fresh vegetables, dairy products as well as
72 yeast.[16,17] It is also extensively used as a component of vitamin preparations and parenteral
73 nutrition solutions.[14,17,18] Dietary deficiency, although uncommon, manifests itself by
74 disturbances of the skin and eyes.[15,17] Being also an essential component of many bodily
75 enzymes and coenzymes, vitamin B_2 proved to be vital to the normal functioning of a
76 number of systemic oxidation-reduction reactions as well as several metabolic
77 pathways.[15,16] Furthermore, recent findings have also revealed that Ribo can inactivate high
78 levels of a broad range of viruses and bacteria present in red blood cells, fresh frozen
79 plasma and platelet concentrates.[19,20]

80

81 Ribo is a member of the 7,8-dimethyl substituted isoalloxazines or the flavins family as the
82 molecule consists of an isoalloxazine ring linked to D-ribitol. Although thermally stable, Ribo
83 has long been known to photodegrade with light.[21,22] An extensive number of studies and
84 research papers have been devoted to the photochemistry of Ribo in both aqueous and
85 organic solvents.[21] Its photodegradation was shown to occur sequentially in a two-step
86 consecutive reaction in alcohols and aqueous buffered acidic solutions. It phototransforms
87 into an intermediate formylmethylflavin (FMF) which, in turn, irreversibly photoreacts to
88 produce lumichrome (LC).[23-27] In alkaline solutions, Ribo hydrolysis contributes in rendering
89 the photoreaction mechanism more complex.[23,24,28]

While studies on Ribo photoproducts, photoreactions mechanisms and to some extent photostabilising means are abundant, the kinetics of photodegradation reactions have been less appreciably explored. The published kinetic studies on Ribo photodegradation were conducted using classical treatments of thermal reactions and were ascribed the apparent first-order kinetics.[18,23,24]

2. Materials and methods

2.1. Materials

Riboflavin, 10-(2,3,4,5-tetrahydroxypentyl)-7,8-dimethylbenzo[*g*]pteridine-2,4(3*H*,10*H*)-dione), and spectroscopic grade ethanol were purchased from Sigma-Aldrich and used without further purification.

2.2. Methods

2.2.1. Numerical integration method (NIM)

A fifth-order Runge-Kutta (RK-5) numerical integration programme within Mathcad 2.1 software, was used to generate numerical integration data for simulated $AB_4(4\Phi)$ reactions. RK-5 programme was fed with plausible reaction parameters to produce kinetic traces representing the time variation of the species' concentration/absorbance. Such traces were used to test, optimise and then validate the semi-empirical rate-law for $AB_4(4\Phi)$ reactions.

2.2.3. Monochromatic continuous irradiation

An Ushio 1000 W xenon arc–lamp light source housed in a housing shell model A6000 and powered by a power supply model LPS–1200, was used for irradiation experiments. This setting was cooled by tap water circulation through a pipe system. The lamp housing was connected to a monochromator model 101 that allows the selection of specific irradiation wavelenghths since it consists of a special f/2.5 monochromator with a 1200 groove/300 nm blaze grating. The excitation beam was guided through an optical fibre to impinge from the top of the sample cuvette i.e. the excitation and the analysis light beams were perpendicular to each other. The setup was manufactured by Photon Technology International Corporation.

2.2.4. Radiant power meter

An Oriel Radiant Power/Energy meter model 70260 was used to measure the radiant power of the incident excitation beams at a specific wavelength. The radiant power, ($P_{\lambda_{irr}}$), was obtained in mW/cm^2 and later transformed into einstein.s^{-1}.dm^{-3} in order to fit the unit system of the Φ-order equations specially the overall rate constant, $k_{\lambda_{irr}}$.

2.2.5. In-Situ reaction monitoring system

A diode array spectrophotometer (Agilent 8453) was used to measure the various absorption spectra and kinetic profiles for the irradiation and calibration experiments. This spectrophotometer was equipped with a 1–cm cuvette sample holder and a Peltier system model Agilent 8453 for temperature control. As such, the sample was kept at 22°C, stirred continuously during the reaction monitored experiment, and completely shielded from

ambient light. The spectrophotometer was monitored by an Agilent 8453 Chemstation kinetics–software.

2.2.6. Riboflavin solutions

A 1.2 x 10^{-4} M stock solution of Ribo in ethanol was prepared by weighing the solid. The solution flask was protected from light by aluminium foil wrapping and was kept in the fridge. The stock solution was diluted to prepare fresh analytical solutions (*ca.* 1.5 x 10^{-6} M) for analysis of irradiation experiments performed at various wavelengths. Degassing of the solutions was not performed in this study.

For actinometric studies, Ribo solutions of approximately the same concentrations (*ca.* 1.8 x 10^{-6} M) were exposed to specific wavelength irradiations (420, 445, 460 and 480 nm) using a series of different radiant power values for each wavelength. The kinetic traces were monitored at the observation wavelength λ_{obs}= 445 nm, the maximum of the longest wavelength absorption band, and subsequently fitted with the Φ–order equations.

3. Results and discussion

3.1. Kinetic modelling of consecutive photoreactions

The differential equations defining the time variation of the species concentrations $C_A\ (t), C_{B_{1-4}}(t)$ which correspond to reactant A and photoproducts B_{1-4}, respectively (Scheme 1), are given by Eqs.(1). This system of equations was derived considering that the solution is subjected to a monochromatic λ_{irr} continuous irradiation, is homogeneously and

continuously stirred, the medium temperature is constant, the concentration of the excited state species is assumed to be negligible, and at the (non-isosbestic) irradiation wavelength (λ_{irr}), species A and B_{1-4} are characterised by different absorption coefficients ε i.e. they absorb different amounts of light ($P_{\lambda_{irr}}$)

$$\frac{dC_A\ (t)}{dt} = -\Phi_{A\to B_1}^{\lambda_{irr}} \times \varepsilon_A^{\lambda_{irr}} \times l_{\lambda_{irr}} \times P_{\lambda_{irr}} \times F_{\lambda_{irr}}(t) \times C_A\ (t) \qquad (1a)$$

$$\frac{dC_{B_1}(t)}{dt} = \left(\Phi_{A\to B_1}^{\lambda_{irr}} \times \varepsilon_A^{\lambda_{irr}} \times C_A\ (t) - \Phi_{B_1\to B_2}^{\lambda_{irr}} \times \varepsilon_{B_1}^{\lambda_{irr}} \times C_{B_1}(t)\right) \times l_{\lambda_{irr}} \times P_{\lambda_{irr}} \times F_{\lambda_{irr}}(t) \qquad (1b)$$

$$\frac{dC_{B_2}(t)}{dt} = \left(\Phi_{B_1\to B_2}^{\lambda_{irr}} \times \varepsilon_{B_1}^{\lambda_{irr}} \times C_{B_1}(t) - \Phi_{B_2\to B_3}^{\lambda_{irr}} \times \varepsilon_{B_2}^{\lambda_{irr}} \times C_{B_2}(t)\right) \times l_{\lambda_{irr}} \times P_{\lambda_{irr}} \times F_{\lambda_{irr}}(t) \qquad (1c)$$

$$\frac{dC_{B_3}(t)}{dt} = \left(\Phi_{B_2\to B_3}^{\lambda_{irr}} \times \varepsilon_{B_2}^{\lambda_{irr}} \times C_{B_2}(t) - \Phi_{B_3\to B_4}^{\lambda_{irr}} \times \varepsilon_{B_3}^{\lambda_{irr}} \times C_{B_3}(t)\right) \times l_{\lambda_{irr}} \times P_{\lambda_{irr}} \times F_{\lambda_{irr}}(t) \qquad (1d)$$

$$\frac{dC_{B_4}(t)}{dt} = \Phi_{B_3\to B_4}^{\lambda_{irr}} \times \varepsilon_{B_4}^{\lambda_{irr}} \times C_{B_4}(t) \times l_{\lambda_{irr}} \times P_{\lambda_{irr}} \times F_{\lambda_{irr}}(t) \qquad (1e)$$

where $\Phi_{A\to B_1}^{\lambda_{irr}}$, $\Phi_{B_1\to B_2}^{\lambda_{irr}}$, $\Phi_{B_2\to B_3}^{\lambda_{irr}}$ and $\Phi_{B_3\to B_4}^{\lambda_{irr}}$ are the quantum yields of the consecutive photoreaction steps, realised at λ_{irr} (nm). The excitation beam traverses the sample with an optical path-length, $l_{\lambda_{irr}}$ (cm). $\varepsilon_A^{\lambda_{irr}}$, $\varepsilon_{B_{1-4}}^{\lambda_{irr}}$ ($M^{-1}cm^{-1}$), are the molar absorption coefficients of the species and $P_{\lambda_{irr}}$ (einstein.$s^{-1}dm^{-3}$) is the radiant power of the monochromatic beam. $F_{\lambda_{irr}}(t)$, the photokinetic factor, is expressed as,

$$F_{\lambda_{irr}}(t) = \frac{1 - 10^{-\left(A_{tot}^{\lambda_{irr}/\lambda_{irr}}(t) \times \frac{l_{\lambda_{irr}}}{l_{\lambda_{obs}}}\right)}}{A_{tot}^{\lambda_{irr}/\lambda_{irr}}(t) \times \frac{l_{\lambda_{irr}}}{l_{\lambda_{obs}}}} \qquad (2)$$

with $l_{\lambda_{obs}}$(cm) being the path-length of the monitoring light of the spectrophotometer through the sample and $A_{\text{tot}}^{\lambda_{irr}/\lambda_{irr}}(t)$, the total absorbance of the medium irradiated and observed at λ_{irr}.

The mathematical integration of the photoreaction rate-laws (Eqs.(1)) cannot be achieved through closed-form due to the presence of the time-dependent photokinetic factor $F_{\lambda_{irr}}(t)$.

3.1.1. Development of model equations

The methodology previously developed to model the kinetics of unimolecular[12] and reversible[13] photoreactions is employed here for $AB_4(4\Phi)$ reactions. In principle, the method is based on proposing a template set of equations that hold the Φ-order kinetics character in their mathematical formulation (the log-exp function), then modify these equations until a good fitting is obtained for a variety of simulated traces of the studied systems, that were independently generated by Runge-Kutta numerical integration (RK-5).

These semi-empirically integrated rate-laws obtained for $AB_4(4\Phi)$ consecutive reactions are

$$C_A(t) = \frac{Log\left(1 + \left(10^{\left|\varepsilon_A^{\lambda_{irr}} - \varepsilon_{B_1}^{\lambda_{irr}}\right| \times l_{\lambda_{irr}} \times C_A(0)} - 1\right) \times e^{-k_{A\to B_1}^{\lambda_{irr}} \times t}\right)}{\left|\varepsilon_A^{\lambda_{irr}} - \varepsilon_{B_1}^{\lambda_{irr}}\right| \times l_{\lambda_{irr}}} \qquad (3a)$$

$$C_{B_1}(t) = \frac{k_{\mathrm{A}\to B_1}^{\lambda_{irr}}}{\left|\varepsilon_A^{\lambda_{irr}} - \varepsilon_{B_1}^{\lambda_{irr}}\right| \times (k_{B_1\to B_2}^{\lambda_{irr}} - k_{\mathrm{A}\to B_1}^{\lambda_{irr}}) \times l_{\lambda_{irr}}} \times \left[Log\left(1 + \left(10^{\left|\varepsilon_A^{\lambda_{irr}} - \varepsilon_{B_1}^{\lambda_{irr}}\right| \times l_{\lambda_{irr}} \times C_A(0)} - 1\right) \times e^{-k_{\mathrm{A}\to B_1}^{\lambda_{irr}} \times t}\right) - Log\left(1 + \left(10^{\left|\varepsilon_A^{\lambda_{irr}} - \varepsilon_{B_1}^{\lambda_{irr}}\right| \times l_{\lambda_{irr}} \times C_A(0)} - 1\right) \times e^{-k_{B_1\to B_2}^{\lambda_{irr}} \times t}\right)\right] \quad (3b)$$

$$C_{B_2}(t) = \frac{k_{\mathrm{A}\to B_1}^{\lambda_{irr}} \times k_{B_1\to B_2}^{\lambda_{irr}}}{\left|\varepsilon_A^{\lambda_{irr}} - \varepsilon_{B_1}^{\lambda_{irr}}\right| \times l_{\lambda_{irr}}} \times \left[\frac{Log\left(1 + \left(10^{\left|\varepsilon_A^{\lambda_{irr}} - \varepsilon_{B_1}^{\lambda_{irr}}\right| \times l_{\lambda_{irr}} \times C_A(0)} - 1\right) \times e^{-k_{\mathrm{A}\to B_1}^{\lambda_{irr}} \times t}\right)}{\left(k_{B_1\to B_2}^{\lambda_{irr}} - k_{\mathrm{A}\to B_1}^{\lambda_{irr}}\right) \times \left(k_{B_2\to B_3}^{\lambda_{irr}} - k_{\mathrm{A}\to B_1}^{\lambda_{irr}}\right)} - \frac{Log\left(1 + \left(10^{\left|\varepsilon_A^{\lambda_{irr}} - \varepsilon_{B_1}^{\lambda_{irr}}\right| \times l_{\lambda_{irr}} \times C_A(0)} - 1\right) \times e^{-k_{B_1\to B_2}^{\lambda_{irr}} \times t}\right)}{\left(k_{B_1\to B_2}^{\lambda_{irr}} - k_{\mathrm{A}\to B_1}^{\lambda_{irr}}\right) \times \left(k_{B_2\to B_3}^{\lambda_{irr}} - k_{B_1\to B_2}^{\lambda_{irr}}\right)} + \frac{Log\left(1 + \left(10^{\left|\varepsilon_A^{\lambda_{irr}} - \varepsilon_{B_1}^{\lambda_{irr}}\right| \times l_{\lambda_{irr}} \times C_A(0)} - 1\right) \times e^{-k_{B_2\to B_3}^{\lambda_{irr}} \times t}\right)}{\left(k_{B_2\to B_3}^{\lambda_{irr}} - k_{B_1\to B_2}^{\lambda_{irr}}\right) \times \left(k_{B_2\to B_3}^{\lambda_{irr}} - k_{\mathrm{A}\to B_1}^{\lambda_{irr}}\right)} \right] \quad (3c)$$

183

$$C_{B_3}(t) = \frac{k_{\mathrm{A}\to \mathrm{B1}}^{\lambda_{irr}} \times k_{\mathrm{B1}\to \mathrm{B2}}^{\lambda_{irr}} \times k_{\mathrm{B2}\to \mathrm{B3}}^{\lambda_{irr}}}{\left|\varepsilon_A^{\lambda_{irr}} - \varepsilon_{B1}^{\lambda_{irr}}\right| \times l_{\lambda_{irr}}} \times$$

$$\left[\frac{Log\left(1 + \left(10^{\left|\varepsilon_A^{\lambda_{irr}} - \varepsilon_{B1}^{\lambda_{irr}}\right| \times l_{\lambda_{irr}} \times C_A(0)} - 1\right) \times e^{-k_{\mathrm{A}\to \mathrm{B1}}^{\lambda_{irr}} \times t}\right)}{(k_{\mathrm{B3}\to \mathrm{B4}}^{\lambda_{irr}} - k_{\mathrm{A}\to \mathrm{B1}}^{\lambda_{irr}}) \times (k_{\mathrm{B1}\to \mathrm{B2}}^{\lambda_{irr}} - k_{\mathrm{A}\to \mathrm{B1}}^{\lambda_{irr}}) \times (k_{\mathrm{B2}\to \mathrm{B3}}^{\lambda_{irr}} - k_{\mathrm{A}\to \mathrm{B1}}^{\lambda_{irr}})} - \frac{Log\left(1 + \left(10^{\left|\varepsilon_A^{\lambda_{irr}} - \varepsilon_{B1}^{\lambda_{irr}}\right| \times l_{\lambda_{irr}} \times C_A(0)} - 1\right) \times e^{-k_{\mathrm{B1}\to \mathrm{B2}}^{\lambda_{irr}} \times t}\right)}{(k_{\mathrm{B1}\to \mathrm{B2}}^{\lambda_{irr}} - k_{\mathrm{A}\to \mathrm{B1}}^{\lambda_{irr}}) \times (k_{\mathrm{B2}\to \mathrm{B3}}^{\lambda_{irr}} - k_{\mathrm{B1}\to \mathrm{B2}}^{\lambda_{irr}}) \times (k_{\mathrm{B3}\to \mathrm{B4}}^{\lambda_{irr}} - k_{\mathrm{B1}\to \mathrm{B2}}^{\lambda_{irr}})} + \frac{Log\left(1 + \left(10^{\left|\varepsilon_A^{\lambda_{irr}} - \varepsilon_{B1}^{\lambda_{irr}}\right| \times l_{\lambda_{irr}} \times C_A(0)} - 1\right) \times e^{-k_{\mathrm{B2}\to \mathrm{B3}}^{\lambda_{irr}} \times t}\right)}{(k_{\mathrm{B2}\to \mathrm{B3}}^{\lambda_{irr}} - k_{\mathrm{A}\to \mathrm{B1}}^{\lambda_{irr}}) \times (k_{\mathrm{B2}\to \mathrm{B3}}^{\lambda_{irr}} - k_{\mathrm{B1}\to \mathrm{B2}}^{\lambda_{irr}}) \times (k_{\mathrm{B3}\to \mathrm{B4}}^{\lambda_{irr}} - k_{\mathrm{B2}\to \mathrm{B3}}^{\lambda_{irr}})} + \frac{Log\left(1 + \left(10^{\left|\varepsilon_A^{\lambda_{irr}} - \varepsilon_{B1}^{\lambda_{irr}}\right| \times l_{\lambda_{irr}} \times C_A(0)} - 1\right) \times e^{-k_{\mathrm{B3}\to \mathrm{B4}}^{\lambda_{irr}} \times t}\right)}{(k_{\mathrm{B1}\to \mathrm{B2}}^{\lambda_{irr}} - k_{\mathrm{A}\to \mathrm{B1}}^{\lambda_{irr}}) \times (k_{\mathrm{B2}\to \mathrm{B3}}^{\lambda_{irr}} - k_{\mathrm{B1}\to \mathrm{B2}}^{\lambda_{irr}}) \times (k_{\mathrm{B3}\to \mathrm{B4}}^{\lambda_{irr}} - k_{\mathrm{B1}\to \mathrm{B2}}^{\lambda_{irr}})} - \frac{Log\left(1 + \left(10^{\left|\varepsilon_A^{\lambda_{irr}} - \varepsilon_{B1}^{\lambda_{irr}}\right| \times l_{\lambda_{irr}} \times C_A(0)} - 1\right) \times e^{-k_{\mathrm{B3}\to \mathrm{B4}}^{\lambda_{irr}} \times t}\right)}{(k_{\mathrm{B3}\to \mathrm{B4}}^{\lambda_{irr}} - k_{\mathrm{A}\to \mathrm{B1}}^{\lambda_{irr}}) \times (k_{\mathrm{B1}\to \mathrm{B2}}^{\lambda_{irr}} - k_{\mathrm{A}\to \mathrm{B1}}^{\lambda_{irr}}) \times (k_{\mathrm{B2}\to \mathrm{B3}}^{\lambda_{irr}} - k_{\mathrm{A}\to \mathrm{B1}}^{\lambda_{irr}})} - \frac{Log\left(1 + \left(10^{\left|\varepsilon_A^{\lambda_{irr}} - \varepsilon_{B1}^{\lambda_{irr}}\right| \times l_{\lambda_{irr}} \times C_A(0)} - 1\right) \times e^{-k_{\mathrm{B3}\to \mathrm{B4}}^{\lambda_{irr}} \times t}\right)}{(k_{\mathrm{B2}\to \mathrm{B3}}^{\lambda_{irr}} - k_{\mathrm{A}\to \mathrm{B1}}^{\lambda_{irr}}) \times (k_{\mathrm{B2}\to \mathrm{B3}}^{\lambda_{irr}} - k_{\mathrm{B1}\to \mathrm{B2}}^{\lambda_{irr}}) \times (k_{\mathrm{B3}\to \mathrm{B4}}^{\lambda_{irr}} - k_{\mathrm{B2}\to \mathrm{B3}}^{\lambda_{irr}})} \right] \quad (3d)$$

$$
\begin{aligned}
&C_{B_4}(t) \\
&= \frac{Log\left(1+\left(10^{\left|\varepsilon_A^{\lambda_{irr}}-\varepsilon_{B1}^{\lambda_{irr}}\right|\times l_{\lambda_{irr}}\times C_A(0)}-1\right)\times e^{-k_{\mathrm{B3\to B4}}^{\lambda_{irr}}\times t}\right)-log\left(10^{\left|\varepsilon_A^{\lambda_{irr}}-\varepsilon_{B1}^{\lambda_{irr}}\right|\times l_{\lambda_{irr}}\times C_A(0)}\right)}{\left|\varepsilon_A^{\lambda_{irr}}-\varepsilon_{B1}^{\lambda_{irr}}\right|\times l_{\lambda_{irr}}} \\
&\times\left[\frac{k_{\mathrm{A\to B1}}^{\lambda_{irr}}\times k_{\mathrm{B1\to B2}}^{\lambda_{irr}}\times k_{\mathrm{B2\to B3}}^{\lambda_{irr}}}{(k_{\mathrm{B3\to B4}}^{\lambda_{irr}}-k_{\mathrm{A\to B1}}^{\lambda_{irr}})\times(k_{\mathrm{B1\to B2}}^{\lambda_{irr}}-k_{\mathrm{A\to B1}}^{\lambda_{irr}})\times(k_{\mathrm{B2\to B3}}^{\lambda_{irr}}-k_{\mathrm{A\to B1}}^{\lambda_{irr}})}\right. \\
&-\frac{k_{\mathrm{A\to B1}}^{\lambda_{irr}}\times k_{\mathrm{B1\to B2}}^{\lambda_{irr}}\times k_{\mathrm{B2\to B3}}^{\lambda_{irr}}}{(k_{\mathrm{B1\to B2}}^{\lambda_{irr}}-k_{\mathrm{A\to B1}}^{\lambda_{irr}})\times(k_{\mathrm{B2\to B3}}^{\lambda_{irr}}-k_{\mathrm{B1\to B2}}^{\lambda_{irr}})\times(k_{\mathrm{B3\to B4}}^{\lambda_{irr}}-k_{\mathrm{B1\to B2}}^{\lambda_{irr}})} \\
&\left.+\frac{k_{\mathrm{A\to B1}}^{\lambda_{irr}}\times k_{\mathrm{B1\to B2}}^{\lambda_{irr}}\times k_{\mathrm{B2\to B3}}^{\lambda_{irr}}}{(k_{\mathrm{B2\to B3}}^{\lambda_{irr}}-k_{\mathrm{A\to B1}}^{\lambda_{irr}})\times(k_{\mathrm{B2\to B3}}^{\lambda_{irr}}-k_{\mathrm{B1\to B2}}^{\lambda_{irr}})\times(k_{\mathrm{B3\to B4}}^{\lambda_{irr}}-k_{\mathrm{B2\to B3}}^{\lambda_{irr}})}\right] \\
&+\frac{k_{\mathrm{B1\to B2}}^{\lambda_{irr}}\times k_{\mathrm{B2\to B3}}^{\lambda_{irr}}\times k_{\mathrm{B3\to B4}}^{\lambda_{irr}}\times Log\left(1+\left(10^{\left|\varepsilon_A^{\lambda_{irr}}-\varepsilon_{B1}^{\lambda_{irr}}\right|\times l_{\lambda_{irr}}\times C_A(0)}-1\right)\times e^{-k_{\mathrm{A\to B1}}^{\lambda_{irr}}\times t}\right)-log\left(10^{\left|\varepsilon_A^{\lambda_{irr}}-\varepsilon_{B1}^{\lambda_{irr}}\right|\times l_{\lambda_{irr}}\times C_A(0)}\right)}{\left|\varepsilon_A^{\lambda_{irr}}-\varepsilon_{B1}^{\lambda_{irr}}\right|\times l_{\lambda_{irr}}\times(k_{\mathrm{B3\to B4}}^{\lambda_{irr}}-k_{\mathrm{A\to B1}}^{\lambda_{irr}})\times(k_{\mathrm{B1\to B2}}^{\lambda_{irr}}-k_{\mathrm{A\to B1}}^{\lambda_{irr}})\times(k_{\mathrm{B2\to B3}}^{\lambda_{irr}}-k_{\mathrm{A\to B1}}^{\lambda_{irr}})} \\
&+\frac{k_{\mathrm{A\to B1}}^{\lambda_{irr}}\times k_{\mathrm{B2\to B3}}^{\lambda_{irr}}\times k_{\mathrm{B3\to B4}}^{\lambda_{irr}}\times Log\left(1+\left(10^{\left|\varepsilon_A^{\lambda_{irr}}-\varepsilon_{B1}^{\lambda_{irr}}\right|\times l_{\lambda_{irr}}\times C_A(0)}-1\right)\times e^{-k_{\mathrm{B1\to B2}}^{\lambda_{irr}}\times t}\right)-log\left(10^{\left|\varepsilon_A^{\lambda_{irr}}-\varepsilon_{B1}^{\lambda_{irr}}\right|\times l_{\lambda_{irr}}\times C_A(0)}\right)}{\left|\varepsilon_A^{\lambda_{irr}}-\varepsilon_{B1}^{\lambda_{irr}}\right|\times l_{\lambda_{irr}}\times(k_{\mathrm{B1\to B2}}^{\lambda_{irr}}-k_{\mathrm{A\to B1}}^{\lambda_{irr}})\times(k_{\mathrm{B2\to B3}}^{\lambda_{irr}}-k_{\mathrm{B1\to B2}}^{\lambda_{irr}})\times(k_{\mathrm{B3\to B4}}^{\lambda_{irr}}-k_{\mathrm{B1\to B2}}^{\lambda_{irr}})} \\
&-\frac{k_{\mathrm{A\to B1}}^{\lambda_{irr}}\times k_{\mathrm{B1\to B2}}^{\lambda_{irr}}\times k_{\mathrm{B3\to B4}}^{\lambda_{irr}}\times Log\left(1+\left(10^{\left|\varepsilon_A^{\lambda_{irr}}-\varepsilon_{B1}^{\lambda_{irr}}\right|\times l_{\lambda_{irr}}\times C_A(0)}-1\right)\times e^{-k_{\mathrm{B2\to B3}}^{\lambda_{irr}}\times t}\right)-log\left(10^{\left|\varepsilon_A^{\lambda_{irr}}-\varepsilon_{B1}^{\lambda_{irr}}\right|\times l_{\lambda_{irr}}\times C_A(0)}\right)}{\left|\varepsilon_A^{\lambda_{irr}}-\varepsilon_{B1}^{\lambda_{irr}}\right|\times l_{\lambda_{irr}}\times(k_{\mathrm{B2\to B3}}^{\lambda_{irr}}-k_{\mathrm{A\to B1}}^{\lambda_{irr}})\times(k_{\mathrm{B2\to B3}}^{\lambda_{irr}}-k_{\mathrm{B1\to B2}}^{\lambda_{irr}})\times(k_{\mathrm{B3\to B4}}^{\lambda_{irr}}-k_{\mathrm{B2\to B3}}^{\lambda_{irr}})}
\end{aligned}
\qquad (3e)
$$

184

185 The general form of the rate-constants $k_{\mathrm{i\to j}}^{\lambda_{irr}}$ (expressed in s^{-1}) is given in Eq.(4) where *i*
186 corresponds to the reacting species in a given reaction step (either the initial reactant or
187 photoproduct) and *j* represents its subsequent photoproduct. β (einstein^{-1} dm^3) is the
188 *pseudo*-rate-constant.[29]

189

$$
k_{\mathrm{i\to j}}^{\lambda_{irr}} = \Phi_{\mathrm{i\to j}}^{\lambda_{irr}}\times\varepsilon_{\mathrm{i}}^{\lambda_{irr}}\times l_{\lambda_{irr}}\times\frac{1-10^{-\varepsilon_{\mathrm{i}}^{\lambda_{irr}}\times l_{\lambda_{irr}}\times C_A(0)}}{\varepsilon_{\mathrm{i}}^{\lambda_{irr}}\times l_{\lambda_{irr}}\times C_A(0)}\times P_{\lambda_{irr}} = \beta_{\mathrm{i\to j}}^{\lambda_{irr}}\times P_{\lambda_{irr}} \qquad (4)
$$

190

191 As the spectroscopic monitoring of the photoreaction offers the cumulative absorbance
192 evolution traces for the medium, rather than the individual species concentrations involved

in the photoreaction, the equation describing the variation of the total absorbance with reaction time for $AB_4(4\Phi)$, is defined on the basis of the individual species time-concentration equations Eq.(3), as

$$A_{\mathrm{Tot}}^{\lambda_{irr}/\lambda_{obs}}(t) = \sum (C_i(t) \times \varepsilon_i^{\lambda_{obs}} \times l_{\lambda_{obs}}) \qquad (5)$$

This model equation offers then the possibility to monitor the evolution of a given consecutive $AB_4(4\Phi)$ photoreaction (or its submechanisms) by using simple UV/Vis spectrophotometric data of the reaction.

It is also interesting to define another important quantity that is accessible from the above equations, namely, the observed initial velocity, $v_o^{\lambda_{irr}/\lambda_{obs}}$ (s^{-1}) of the photoreaction. It can either be worked out from Eqs.(1), as the theoretical equation ($v_{o,\ theo.}^{\lambda_{irr}/\lambda_{obs}}$, Eq.(6a)), or determined from the differentiation of Eq.(5) at the initial time (t = 0), as the formula derived from the model equations ($v_{o,\ mod.}^{\lambda_{irr}/\lambda_{obs}}$, Eq.(6a)) and whose value can be obtained from the traces. The numerical values obtained for both Eqs.(6a) and (6b) should be the same.

$$v_{o,\ theo.}^{\lambda_{irr}/\lambda_{obs}} = \left(\varepsilon_B^{\lambda_{obs}} - \varepsilon_A^{\lambda_{obs}}\right) \times l_{\lambda_{obs}} \times \Phi_{A\rightarrow B_1}^{\lambda_{irr}} \times \varepsilon_A^{\lambda_{irr}} \times l_{\lambda_{irr}} \times P_{\lambda_{irr}} \times F_{\lambda_{irr}}(0) \times C_A\ (0)$$

$$= \delta_{\lambda_{irr}} \times P_{\lambda_{irr}} \qquad (6a)$$

$$\upsilon_{o,\ mod.}^{\lambda_{irr}/\lambda_{obs}} = \frac{l_{\lambda_{obs}} \times k_{\mathrm{A}\to B_1}^{\lambda_{irr}}}{l_{\lambda_{irr}} \times \ln(10)} \times \left(1 - 10^{-\left(\left|\varepsilon_A^{\lambda_{irr}} - \varepsilon_{B_1}^{\lambda_{irr}}\right| \times l_{\lambda_{irr}} \times C_A\,(0)\right)}\right) \qquad (6b)$$

210

211 with $C_A\ (0)$ being the initial concentration of species A and $F_{\lambda_{irr}}(0)$, the photokinetic factor
212 at t = 0 (i.e. in Eq.2, $A_{tot}^{\lambda_{irr}/\lambda_{irr}}(t) = A_A^{\lambda_{irr}/\lambda_{irr}}(0)$).

213

214 It is worth noting that in the case where only one photoreaction step is involved in the
215 reaction (i.e. $k_{B_1\to B_2}^{\lambda_{irr}} = k_{B_2\to B_3}^{\lambda_{irr}} = k_{B_3\to B_4}^{\lambda_{irr}} = 0$), these sets of equations reduce down to the
216 already established equations for AB(1Φ) that have been obtained by closed-form
217 integration.[9]

218

219 **3.1.2. Test and validation of the model equations**

220 The accuracy of the above equations to describe the kinetic evolution of species involved in
221 consecutive photoreactions types was tested against 150 RK-5-generated kinetic traces.
222 These traces were obtained by varying input parameters that fed the RK-5 calculation with
223 plausible values for the $AB_4(4\Phi)$ reactions including initial concentration, $C_A(0)$, radiant
224 power, $P_{\lambda_{irr}}$, irradiation optical path-length, $l_{\lambda_{irr}}$, reactant and photoproducts' absorption
225 coefficients, $\varepsilon^{\lambda_{irr}}$, and photoreaction-steps' quantum yields, $\Phi^{\lambda_{irr}}$. The different simulation
226 scenarios were carefully selected to provide a wide array of reaction eventualities, Table 1
227 (Supplementary data).

228

The proposed general semi-empirical model equation (Eq.5) was found to adequately fit the full set of RK-5 synthetic kinetic traces. The correspondence was found for cases where the photokinetic factor, $F_{\lambda_{irr}}(\infty)$ value measured at the end of the reaction (t = ∞), was equal to or exceeding 1.8 (i.e. $A^{\lambda_{irr}/\lambda_{obs}}(\infty) < 0.22$); a limitation that can usually be circumvented by reducing the initial species concentration or the irradiation optical path-length.

Table 1: Examples of data sets used to generate $AB_4(4\Phi)$ kinetic traces using RK-5. The calculated overall rate-constants values are also indicated.

	Trace 1	Trace 2	Trace 3	Trace 4	Trace 5	Trace 6	Trace 7
$C_A(0) \times 10^6$ (M)	10	8.0	4.0	8.0	9.0	7.0	4.0
$P \times 10^6$ (einstein. $s^{-1}.cm^{-3}$)	5.0	3.0	5.0	6.0	8.0	6.0	7.0
$l_{\lambda_{irr}}$(cm)	1	2.5	5	1.4	1	2	2
$\varepsilon_A^{\lambda_{irr}}$ ($M^{-1}cm^{-1}$)	3500	5500	16000	2500	8550	2200	3750
$\varepsilon_{B_1}^{\lambda_{irr}}$ ($M^{-1}cm^{-1}$)	5800	3200	14000	12400	6500	6500	4800
$\varepsilon_{B_2}^{\lambda_{irr}}$ ($M^{-1}cm^{-1}$)	5900	1500	12000	1100	4200	8700	6700
$\varepsilon_{B_3}^{\lambda_{irr}}$ ($M^{-1}cm^{-1}$)	6300	3666	10000	5000	3100	5000	3200
$\varepsilon_{B_4}^{\lambda_{irr}}$ ($M^{-1}cm^{-1}$)	7000	5700	8000	4000	2249	1050	2100
$\Phi_{A\rightarrow B_1}^{\lambda_{irr}}$	0.1	0.02	0.03	0.1	0.01	0.05	0.02
$\Phi_{B_1\rightarrow B_2}^{\lambda_{irr}}$	0.2	0.1	0.001	0.1	0.2	0.03	0.08
$\Phi_{B_2\rightarrow B_3}^{\lambda_{irr}}$	0.3	0.1	0.02	0.1	0.2	0.01	0.1
$\Phi_{B_3\rightarrow B_4}^{\lambda_{irr}}$	0.1	0.05	0.06	0.1	0.1	0.02	0.05
$k_{A\rightarrow B_1}^{\lambda_{irr}}$ (s^{-1})	0.00387	0.00175	0.01955	0.00490	0.00155	0.00290	0.00234
$k_{B_1\rightarrow B_2}^{\lambda_{irr}}$ (s^{-1})	0.01250	0.00495	0.00059	0.02300	0.02270	0.00520	0.01185
$k_{B_2\rightarrow B_3}^{\lambda_{irr}}$ (s^{-1})	0.01905	0.00230	0.01061	0.00230	0.01510	0.00240	0.02032
$k_{B_3\rightarrow B_4}^{\lambda_{irr}}$ (s^{-1})	0.00675	0.00320	0.02768	0.00900	0.00480	0.00255	0.00501

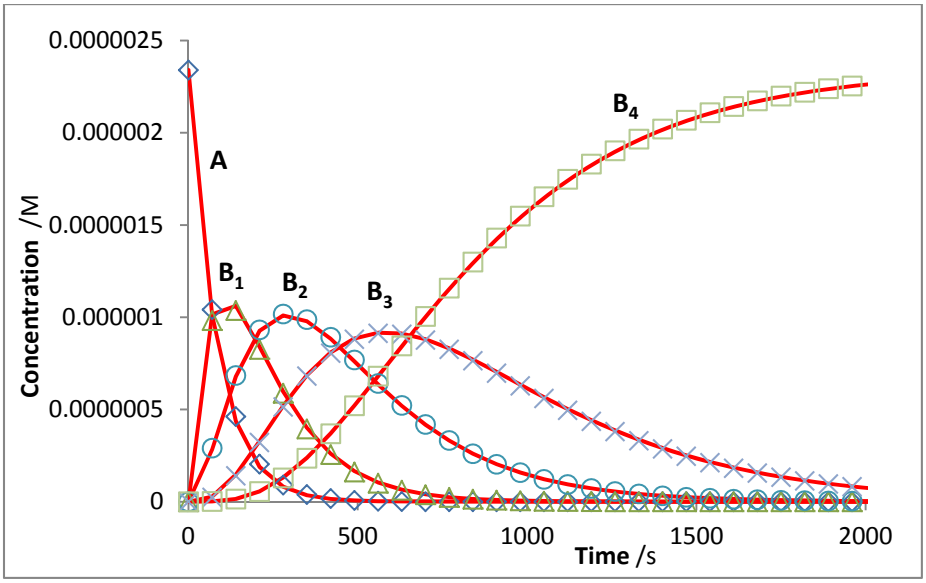

Figure 1: Individual concentration evolution profiles of reactant (A) and photoproducts ($B_{1\text{-}4}$) corresponding to the data of trace 6 in Table 1. The geometric shapes represent the species RK-5 obtained concentrations profiles whereas the continuous lines correspond to fittings with the Φ-order semi-empirical equations, Eqs.(3).

The traces corresponding to the variation of the $AB_4(4\Phi)$ medium absorbance with time can have various shapes depending on individual species' and reactions' parameters (Fig.2). It is therefore not obvious to decide on the mechanism of the reaction solely on the basis of the trace's shape as not all the reaction regimes are evidenced (e.g. Trace #1 in Fig.2 could be confused with an $AB(1\Phi)$ reaction). In any case, it is important to underline that, for the whole RK-5 set of studies, a good fit was obtained for these absorbance traces with the general model Eq.(5). Cases of submechanisms ($AB_3(3\Phi)$ and $AB_2(2\Phi)$) were also successfully tested with reduced Eq.5 (where $k^{\lambda_{irr}}_{B_3 \rightarrow B_4} = 0$ and $k^{\lambda_{irr}}_{B_3 \rightarrow B_4} = k^{\lambda_{irr}}_{B_2 \rightarrow B_3} = 0$, respectively). All of these fitting-tests strengthen the applicability of the equations proposed and their usefulness (Eqs. (3) and (5)).

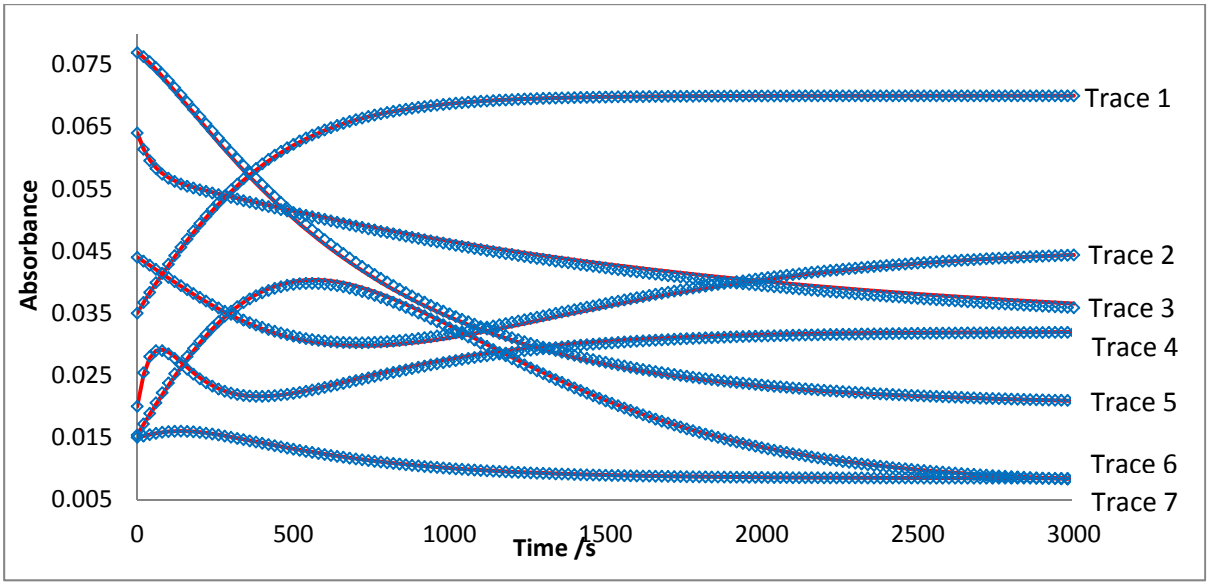

Figure 2: A sample of Runge-Kutta generated $AB_4(4\Phi)$ kinetic traces (circles) and the corresponding $AB_4(4\Phi)$-model (Eq.(5)) fitting traces (lines).

Although necessary, a good fit does not though amount, on its own, to a definite proof of the validity of an equation, as it has been previously discussed.[12] For instance, the $AB_4(4\Phi)$ Trace #1 shown in Fig.1 could well be fitted with the equations corresponding to an $AB(1\Phi)$ reaction. In this respect the methodology imposes that the validation of the equations includes the testing of other parameters by calculating their theoretical values and comparing them to their values obtained from the fitting of the traces.

The first of these parameters is the overall rate-constant. For the 150 cases, Eq.(4) served to calculate the theoretical values, for each individual photoreaction step in a given reaction ($k_{cal.}^{\lambda_{irr}}$), using the data provided in Table 1. Besides, the values of the same overall rate-constants were worked out from the fitting of Eq.(5) to kinetic traces built from the cumulative absorbance of the medium (in this case, the data of Table 1 were supposed not known, except for the experimentally accessible parameters of the initial species). For each

trace, four overall rate-constant values ($k_{mod.}^{\lambda_{irr}}$) were determined. When compared, a good linear correlation was found between the two ($k_{mod.}^{\lambda_{irr}}$ and $k_{cal.}^{\lambda_{irr}}$) sets of values (Fig.3A)

The initial velocity values were similarly determined and compared using Eqs.(6) (for $\upsilon_{o\ theo.}^{\lambda_{irr}/\lambda_{obs}}$ and $\upsilon_{o,mod.}^{\lambda_{irr}/\lambda_{obs}}$, respectively). A good fit was evidenced here as well (Fig.3B). Overall, the calculated and model fitting-determined parameter values for both k and υ_o, differed by no more than 10%. The close correlations obtained between the two sets of values (Fig.3) provide validation for the accuracy of the semi-empirical integrated rate-law equations

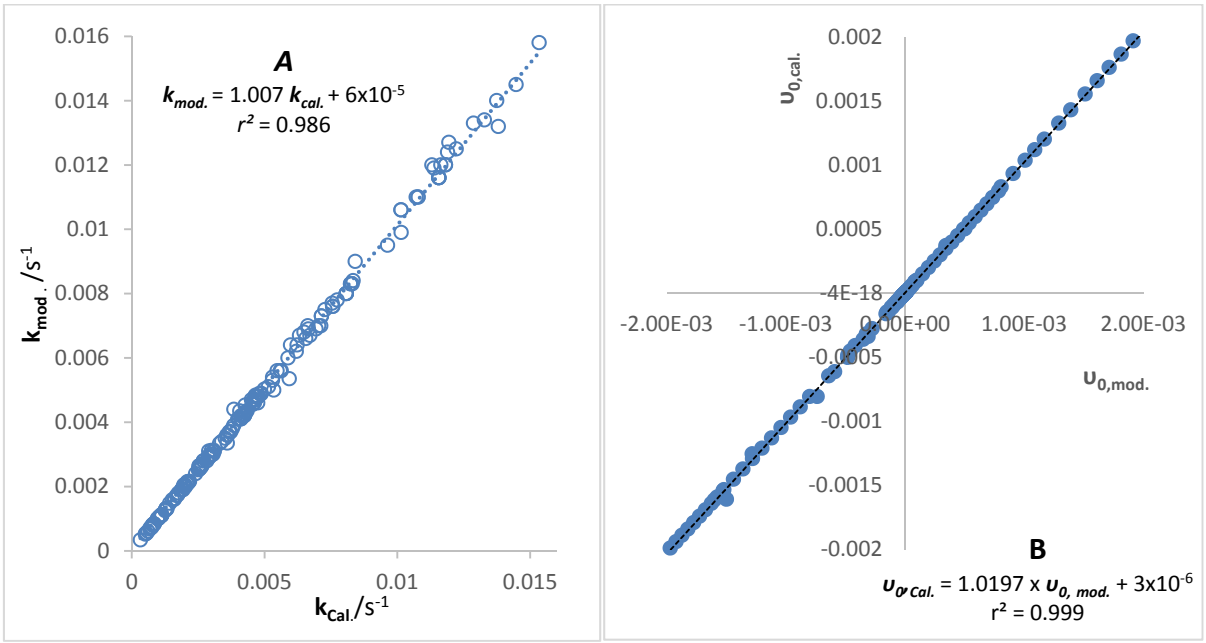

Figure 3: Correlation between the rate-constant ($k_{cld.}^{\lambda_{irr}}$, Fig.3A) and the initial velocity ($\upsilon_{o\ theo.}^{\lambda_{irr}/\lambda_{obs}}$, Fig.3B) values calculated theoretically using the $AB_4(4\Phi)$ Eq.4 and Eq.6a equations respectively), and those determined from the fitting of RK–4 data with the $AB_4(4\Phi)$ model equations, $k_{mod.}^{\lambda_{irr}}$ (Eq.5) and $\upsilon_{o,mod.}^{\lambda_{irr}/\lambda_{obs}}$ (Eq.6b), respectively, for over 150 simulation photokinetic traces.

(Eqs.(3)–(6)) to describe the kinetic evolution of consecutive $AB_4(4\Phi)$ photoreactions (and its submechanisms).

As a result, the above proposed semi-empirical model Eqs.(3)–(6) can be used to investigate experimental photokinetic data.

3.2. Elucidation of Riboflavin photodegradation kinetics

3.2.1. Riboflavin photodegradation

The photodegradation of Ribo in ethanol was reported to occur via the $AB_2(2\Phi)$ consecutive photoreaction mechanism (Scheme 2). An intermediate aldehyde photoproduct, FMF, is formed by intramolecular photoreduction of the isoalloxazine ring system followed by oxidation of the ribityl side-chain. This first photoreaction step was shown to occur predominantly from the triplet state of the photo-excited Ribo molecule.[28,30] It was suggested that the ribityl chain rich in hydroxyl oxygen atoms promotes the transition from the excited singlet to the excited triplet-state and stabilises the latter by steric protection.[28] The intersystem crossing quantum yield for Ribo was reported to be high around 0.6 in methanol[31] and 0.7 in ethanol.[27]. Triplet state lifetimes of 3.7 and 19 µs were also reported for Ribo in aqueous and methanolic solutions, respectively.[32,33] The second photolysis step in Ribo degradation was also reported to occur from the lowest triplet state of the photoactivated FMF which undergoes a redox reaction to generate LC.[25]

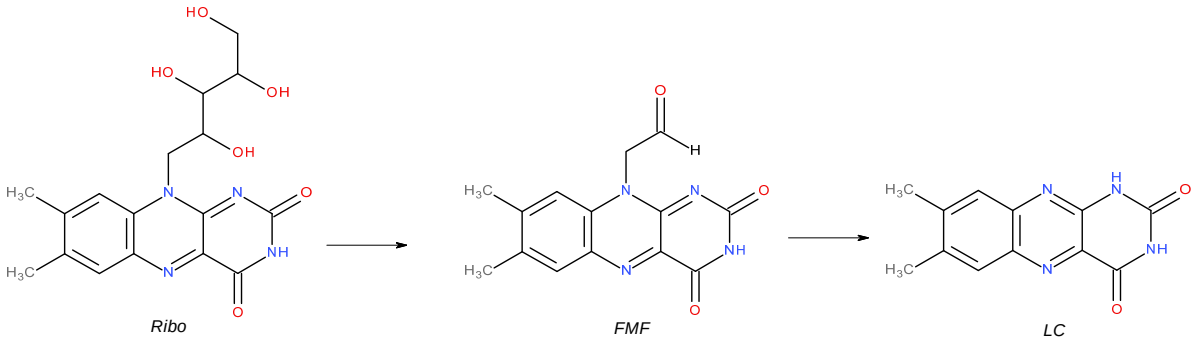

Scheme 2: Consecutive $AB_2(2\Phi)$ photoreaction mechanism of Ribo upon exposure to UV–irradiation.

The electronic absorption spectrum of *Ribo* in ethanol is characterised by four absorption bands spanning the UV and visible regions of the spectrum (Fig.5). Two intense peaks at 220 and 265 nm characterise the lower UV region and two broad absorption bands in UVA-Vis longer wavelengths have maxima at 360 and 445 nm. The absorbance bands in the near UV and visible parts of the spectrum have mainly been attributed to π-π^* transitions.[25,28,32,33] Monochromatic irradiation of Ribo ethanolic solutions resulted in the photobleaching of the solution through the typical disappearance of the visible absorption peak with a concomitant decrease in absorbance in the UV region and the appearance of a shoulder at around 390 nm. The recorded isosbestic points at 405, 383, 320, 303, 260, and 233 nm, characterise the smoothness of the photoreaction (Fig.5). These features also indicate the photodegradation of Ribo in solution and its depletion at long exposure times.

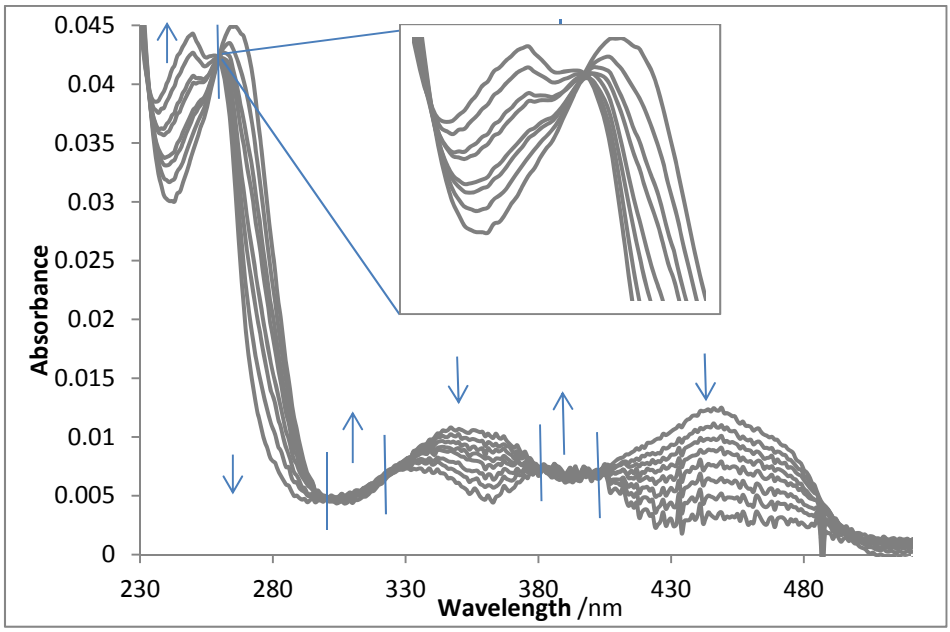

Figure 5: Evolution of the electronic absorption spectra of 1.11 x 10^{-6} M *Riboflavin* in ethanol subjected to continuous irradiation with a 460 nm monochromatic beam (at a radiant power of P_{270} = 1.36 x 10^{-6} einstein.s^{-1}.dm^{-3}) for 4 hours. The arrows indicate the direction of the absorbance evolution during the photoreaction, and the vertical lines cross the spectra at the isosbestic points (405, 383, 320, 303, 260, and 233 nm).

3.2.2. Φ-order photokinetics of Riboflavin

It has been reported that wavelengths in the range of 350-500 nm cause Ribo photodegradation with the wavelength range of 415 – 455 nm being the most damaging.[21] Furthermore, photoirradiation experiments of Ribo in ethanol revealed a considerably slower photoreaction under UVB irradiation compared to irradiations undertaken in the visible region of the spectrum.[21] Accordingly, the present kinetic study was predominantly focused on investigating Ribo photokinetics in the photodegradation causative range situated between 400 and 480 nm.

Monochromatic irradiation experiments were performed at different wavelengths (λ_{irr} = 400, 420, 445, 460 and 480 nm) in order to cover the whole wavelength range of interest.

The changes in absorbance of the medium were monitored at different observation wavelengths (λ_{obs}) including the wavelength of irradiation ($\lambda_{obs} = \lambda_{irr}$ so that $\varepsilon_{B_1}^{\lambda_{irr}} = \varepsilon_{B_1}^{\lambda_{obs}}$), for each irradiation experiment.

Continuous irradiation of Ribo under different wavelengths results in the gradual reduction of absorbance as observed at 445 nm (Fig.6). Fitting of these traces was performed using Eq.(5) where $k_{B_2 \rightarrow B_3}^{\lambda_{irr}}$ and $k_{B_3 \rightarrow B_4}^{\lambda_{irr}}$ in Eq.4 were given the zero value to correspond to the $AB_2(2\Phi)$ mechanism of Ribo.

An accurate fitting of the semi-empirical model, Eq.(5), to the experimental kinetic traces was obtained for all experimental kinetic traces of Ribo photodegradation (irrespective of $\lambda_{irr}/\lambda_{obs}$). This finding further confirms the consecutive $AB_2(2\Phi)$ nature of Ribo photoreaction in ethanol.

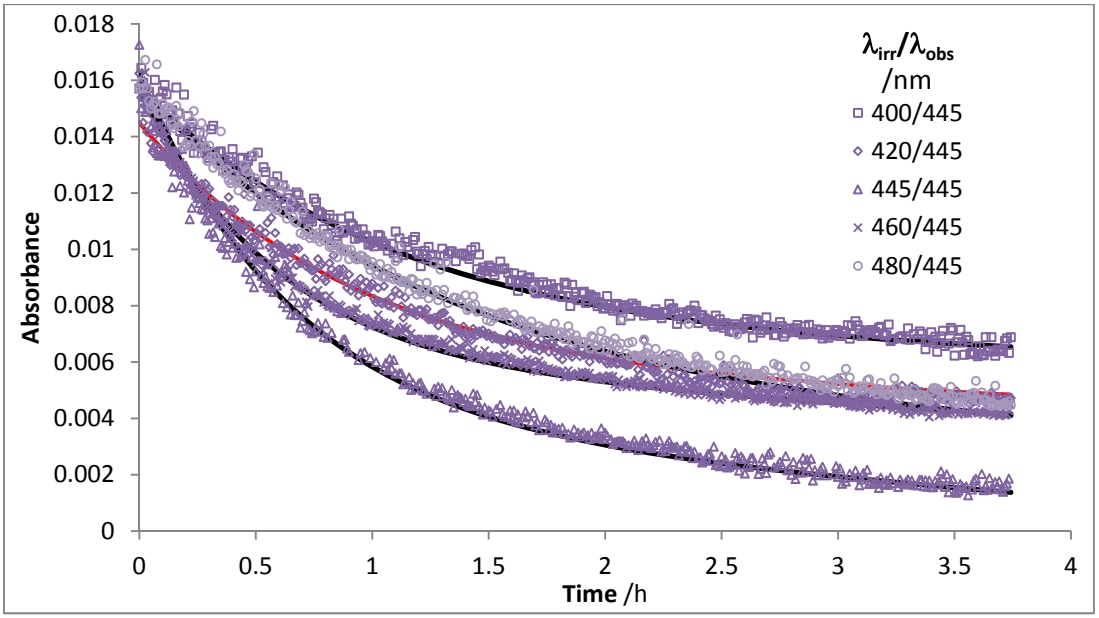

Figure 6: The photokinetic traces for the photodegradation of Ribo in ethanol (~1.2 x 10^{-6} M) under continuous irradiations at λ_{irr}= 400, 420, 445, 460 and 480nm and observation at λ_{obs}= 445nm. The geometric shapes represent the experimental data whereas the continuous lines represent the model fitted traces using Eq.(5).

Fitting of the model allowed the determination of the individual overall rate-constants of the consecutive photoreaction steps, $k_{A\rightarrow B_1}^{\lambda_{irr}}$ and $k_{B_1\rightarrow B_2}^{\lambda_{irr}}$, respectively. $k_{A\rightarrow B_1}^{\lambda_{irr}}$ was found to be 10 to 40–fold higher than $k_{B_1\rightarrow B_2}^{\lambda_{irr}}$ for the 400-480 nm irradiation range, even though both indicate relatively low (0.1–5 10^{-4} s^{-1}) reactivity (Table 2). On the other hand, both overall rate-constant values were found to increase with irradiation wavelength between 400 and 460 nm, reaching their maximum at 460 nm and subsequently decreasing.

If k values can provide indication about individual photoreactions' rates for the experimental conditions used, they do not reflect the photochemical efficiencies of the reactive molecules at the selected irradiation wavelength, nor can they be used to compare photoreaction rates from comparable studies using different experimental conditions or drug molecules. Therefore, a photokinetic elucidation method should be adopted in order to allow the determination of individual photoreaction quantum yields for each step of the $AB_2(2\Phi)$ reactions.

3.2.3. Elucidation of $AB_2(2\Phi)$ photoreaction kinetics

A comprehensive kinetic elucidation of a bimolecular consecutive, $AB_2(2\Phi)$, photoreaction system entails the determination of the absolute values of four parameters, namely; $\varepsilon_{B_1}^{\lambda_{irr}}$, $\varepsilon_{B_2}^{\lambda_{irr}}$, $\Phi_{A\to B_1}^{\lambda_{irr}}$ and $\Phi_{B_1\to B_2}^{\lambda_{irr}}$.

For $AB_2(2\Phi)$ Φ-order kinetic, the elucidation method starts with the determination of the absorption coefficients, $\varepsilon_A^{\lambda_{irr}}$and $\varepsilon_{B_2}^{\lambda_{irr}}$, corresponding to Ribo and its final photoproduct, *LC,* respectively. They are obtained from the initial (t = 0) and final (t = ∞, using Eq.(7a)) absorption spectra of the photodegradation reaction.

$$\varepsilon_{B_2}^{\lambda_{irr}} = \frac{A_{tot}^{\lambda_{irr}/\lambda_{obs}}(\infty)}{l_{\lambda_{obs}} \times C_A\ (0)} \qquad (7a)$$

The quantum yield of the first photoreaction step, $\Phi_{A\to B_1}^{\lambda_{irr}}$, is derived from the value obtained from the fitting and the formula, Eq.(4), of the overall rate-constant, as

$$\Phi_{A\to B_1}^{\lambda_{irr}} = \frac{k_{\mathrm{A}\to B_1}^{\lambda_{irr}} \times A_{tot.}^{\lambda_{irr}/\lambda_{irr}}(0)}{\varepsilon_A^{\lambda_{irr}} \times l_{\lambda_{irr}} \times P_{\lambda_{irr}} \times \left(1 - 10^{-A_{tot.}^{\lambda_{irr}/\lambda_{irr}}(0)}\right)} \qquad (7b)$$

Then, the value of $\varepsilon_{B_1}^{\lambda_{irr}}$ can be calculated from the value, Eq.(6b), and the formula, Eq.(6a) of the initial velocity, $v_o^{\lambda_{irr}/\lambda_{obs}}$, as,

$$\varepsilon_{B_1}^{\lambda_{obs}} = \frac{v_o^{\lambda_{irr}/\lambda_{obs}}}{l_{\lambda_{obs}} \times \Phi_{A\to B_1}^{\lambda_{irr}} \times \varepsilon_A^{\lambda_{irr}} \times l_{\lambda_{irr}} \times P_{\lambda_{irr}} \times F^{\lambda_{irr}/\lambda_{irr}}(0) \times C_A\ (0)} + \varepsilon_A^{\lambda_{obs}} \qquad (7c)$$

Finally, the quantum yield of the second photoreaction step, $\Phi_{B_1 \rightarrow B_2}^{\lambda_{irr}}$, can be determined from the equation and value of the overall rate-constant for the phototransformation of B_1 into B_2 ($k_{B_1 \rightarrow B_2}^{\lambda_{irr}}$) is given by Eq.(7d).

$$\Phi_{B_1 \rightarrow B_2}^{\lambda_{irr}} = \frac{k_{B_1 \rightarrow B_2}^{\lambda_{irr}} \times \varepsilon_{B_1}^{\lambda_{irr}} \times l_{\lambda_{irr}} \times C_A(0)}{\varepsilon_{B_1}^{\lambda_{irr}} \times l_{\lambda_{irr}} \times P_{\lambda_{irr}} \times \left(1 - 10^{-\varepsilon_{B_1}^{\lambda_{irr}} \times l_{\lambda_{irr}} \times C_A(0)}\right)} \qquad (7d)$$

Appling the above elucidation methods to the kinetic data obtained for each individual irradiation wavelength across the selected spectral range allows defining a number of reaction's and species' attributes.

The absorption spectra of the reactive species can be reconstructed. They show that the three compounds are characterised by low absorptivities (< 12000 M^{-1} cm^{-1} for λ > 400 nm) and that only LC (B_2) does not absorb beyond 450 nm (Fig. 7 and Table 2).

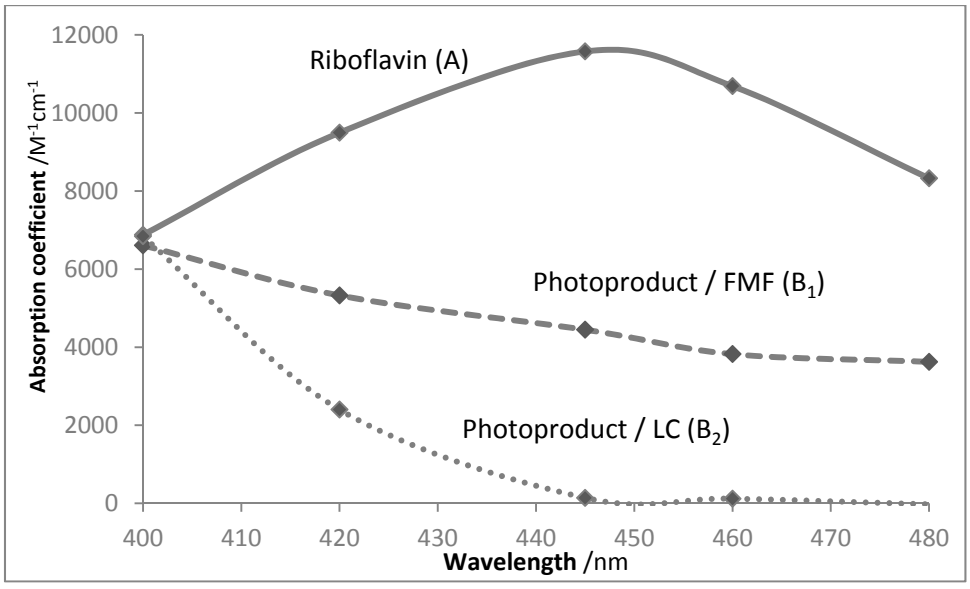

Figure 7: Electronic absorption spectra (expressed as absorption coefficient units) of Riboflavin and its two photoproducts B_1 and B_2.

411 Our results however corroborate those obtained on solutions of the individual species of
412 Ribo and LC in methanol.[34]

413

414 It is also straightforward to retrieve the individual concentration profiles (Fig.8) of A, B_1 and
415 B_2 by substitution of the values of $\varepsilon_A^{\lambda_{irr}}$, $\varepsilon_{B_1}^{\lambda_{irr}}$, $k_{A\rightarrow B_1}^{\lambda_{irr}}$ *and* $k_{B_1\rightarrow B_2}^{\lambda_{irr}}$ into concentration
416 equations, Eqs.(3). It is interesting to notice that Ribo photo-depletion is achieved in the
417 relatively early stages of the reaction (~ 3 hours) compared to its photoproduct. This means
418 that a subtle change of colour is not necessarily indicative of the presence of Ribo in
419 solution.

420

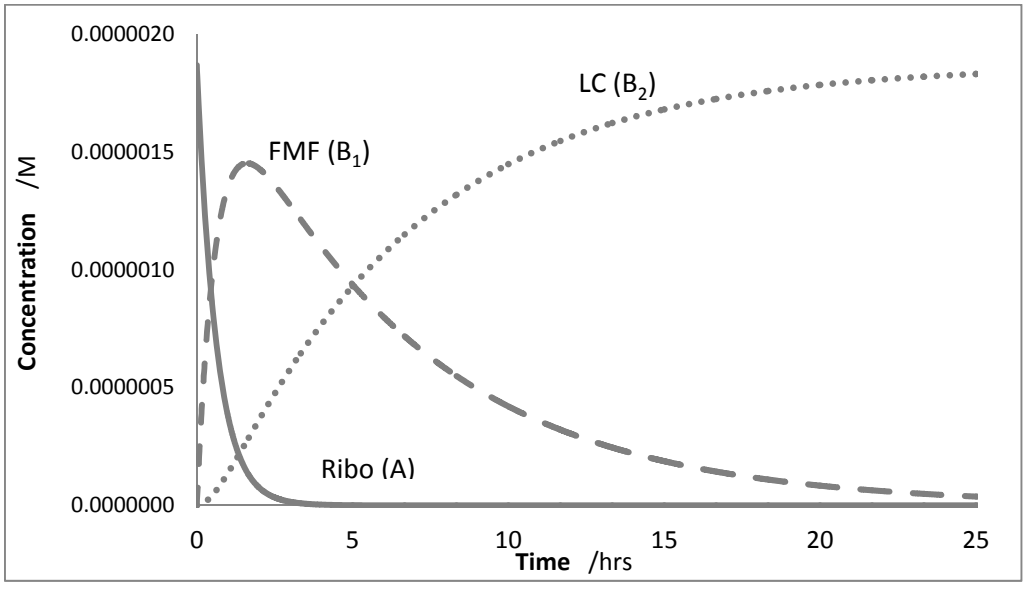

421

422 **Figure 8:** Evolution of the concentration profiles of Ribo (1.8 x 10^{-6} M) and its photoproducts
423 (B_1 and B_2) upon irradiation at 445 nm (P_{445} = 1.26 x 10^{-6} einstein. s^{-1}.dm^{-3}), as determined
424 using the $AB_2(2\Phi)$-model concentration equations (Eqs.3a-3c).

425

426

427

Table 2: Quantum yields, overall rate–constant and absorption coefficient values for *Riboflavin* photodegradation reactions and its two photoproducts measured at various monochromatic and continuous irradiations.

λ_{irr}/nm	$C(0)$ x 10^6 / M	$P_{\lambda_{irr}}$ x 10^6 /einstein.s^{-1}.dm^{-3}	$\varepsilon_A^{\lambda_{irr}}$/$M^{-1}cm^{-1}$	$\varepsilon_{B_1}^{\lambda_{irr}}$/$M^{-1}cm^{-1}$	$\varepsilon_{B_2}^{\lambda_{irr}}$/ M^{-1} cm^{-1}	$k_{A\rightarrow B_1}^{\lambda_{irr}}$ x 10^4 / s^{-1}	$k_{B_1\rightarrow B_2}^{\lambda_{irr}}$ x 10^4 / s^{-1}	$\Phi_{A\rightarrow B_1}^{\lambda_{irr}}$ x 10^2	$\Phi_{B_1\rightarrow B_2}^{\lambda_{irr}}$ x 10^2
400	1.46	1.29	6880	6607	6840	2.4	0.06	0.504±0.0003	0.008±0.001
420	1.03	1.30	9494	5325	2400	3.2	0.22	0.625± 0.021	0.009±0.002
445	1.87	1.26	11578	4447	141	4.7	0.36	0.687±0.027	0.096±0.018
460	1.55	1.39	10685	2822	120	5.1	0.40	0.764±0.012	0.126±0.043
480	1.11	1.39	8325	3625	0	3.5	0.34	0.756±0.118	0.127±0.035

3.3. Wavelength-quantum yield relationship

The individual quantum yield values (Table 2) increased with irradiation wavelength in the visible region of the spectrum (Fig.9). This variation however, was more pronounced for the second photoreaction step (FMF) with a 5-fold increment between the lowest and highest recorded quantum yields compared to only a 1.5-fold variation for the quantum yields corresponding to the initial photoreaction step (Ribo). The quantum yield values $\Phi_{A\rightarrow B_1}^{\lambda_{irr}}$ were 6 – 20 times higher than the subsequent $\Phi_{B_1\rightarrow B_2}^{\lambda_{irr}}$. Interestingly, the variations of both sets of quantum yield values were well described by sigmoid functions (Eqs.8). The sigmoid equations offer the possibility to determine the quantum yields of photoreactions at any wavelength between 400-480 nm based on only a few experimental points. Overall, such kinetic behaviour has previously been observed for several drugs.[12,29,35-38] These findings might suggest a common trend for photodrugs and certainly confirm that the quantum yields must be experimentally defined before any conclusions on their wavelength-independence can be reached.

$$\Phi_{A\rightarrow B_1}^{\lambda_{irr}} = \frac{0.0006}{0.22 + 0.155 \times e^{-0.1(\lambda_{irr}-439.9)}} + 0.004965 \qquad (8a)$$

$$\Phi_{B_1\rightarrow B_2}^{\lambda_{irr}} = \frac{0.0002}{0.18 + 0.13 \times e^{-0.11(\lambda_{irr}-439.9)}} + 0.00019 \qquad (8b)$$

Overall, the quantum yield values for Ribo photodegradation were one order of magnitude smaller than those recorded for nifedipine,[12] nisoldipine,[38] montelukast[35] and fluvoxamine[29], 10- and 100-fold lower than Dacarbazine[36] and Sunitinib, respectively.[37]

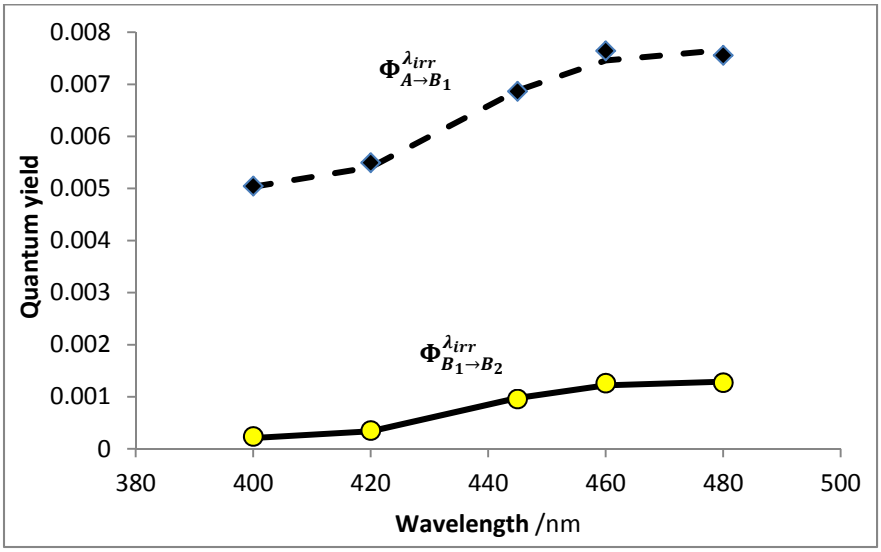

Figure 9: Quantum yield values for the two consecutive photoreaction steps of Ribo (1.8 x 10^{-6} M) photodegradation in ethanol for different irradiation wavelengths (shapes) together with the sigmoid fitted functions, Eqs.8, (lines).

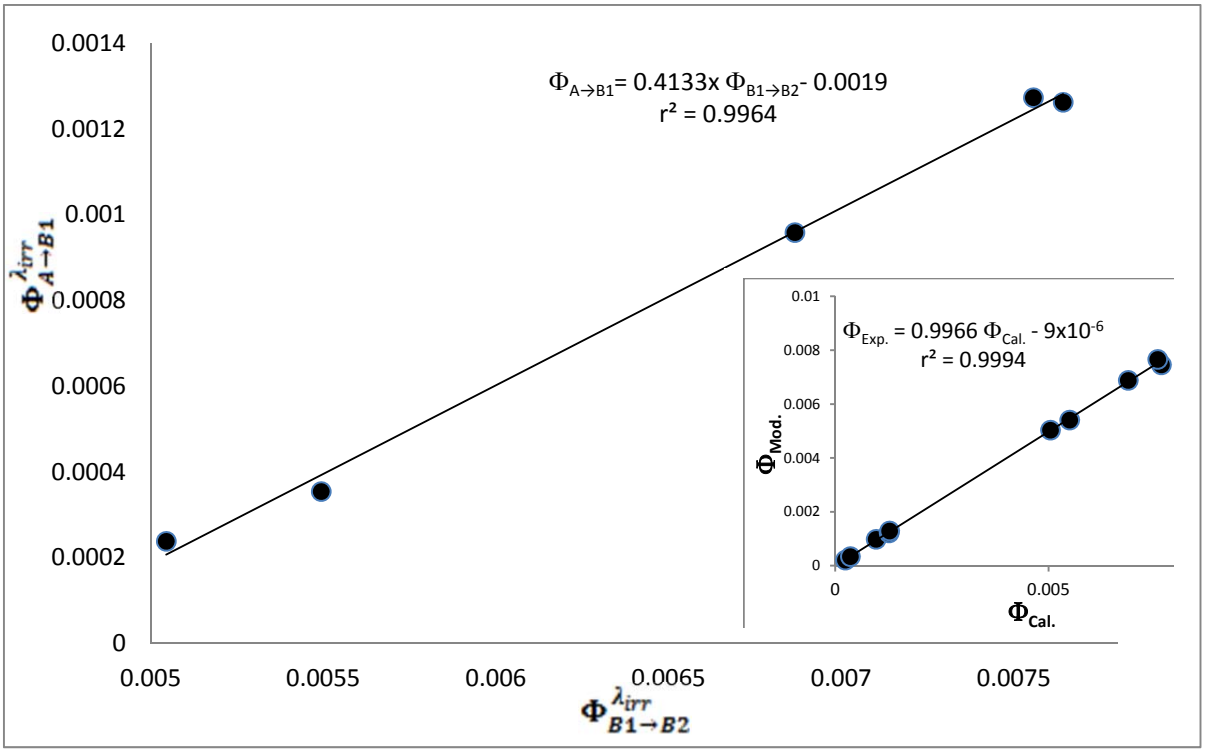

Figure 10: Correlation between experimental quantum yield values corresponding to the first and second photoreaction steps of Ribo photodegradation in ethanol. Inset: Correlation between experimental ($\Phi_{Exp.}$) and calculated ($\Phi_{Cal.}$, Eqs.(8)) quantum yield values for Ribo.

462 Remarkably, a linear correlation could be established between the first and second
463 photoreactions quantum yields values for increasing irradiation wavelengths (Fig.10). This
464 might indicate the important/predominant role of the isoalloxazine ring in the primary
465 photochemical steps of Ribo and FMF (which is also supported by the absence of
466 photoreactivity in the more aromatic LC).

467

468 Different evaluation methods were used for the determination of the photodegradation
469 quantum yield of Ribo as reported in the literature.[40-43] The values ranged between 12 10^{-3}
470 and 7.3 10^{-3} (pH = 7.8) in water[40,41], and 10^{-3} – 10^{-4} and 2 × 10^{-5} in methanolic solutions.[42,43]
471 Overall, these values agree well with our findings that have been obtained in ethanol (3.5–
472 7.5 10^{-3}).

473

474 Over the last 50 years, a substantial number of compounds exhibiting wavelength-
475 dependent quantum yields were reported despite their "normal" features in fluorescence.[44-
476 48] This strongly points to a limitation of a universal applicability of Kasha's rule in
477 photochemical processes, as suggested, in the late 1970s, by Turro *et al.*[49] The literature
478 does not yet provide a general and/or a unique fundamental explanation for the observed
479 phenomenon. We have experimentally observed similar phenomenon for many
480 drugs,[12,29,35-39] that are corroborated by the findings reported in the literature.

481

482

483

3.4. *Pseudo*-constants

The *pseudo*-rate ($\beta_{\lambda_{irr}}$, Eq.(4)) and *pseudo*-initial velocity ($\delta_{\lambda_{irr}}$, Eq.(6a)) constants can be determined by fitting Eq.(5) to the experimental kinetic data obtained for increasing radiant power ($P_{\lambda_{irr}}$) values at λ_{irr} (Fig.11). The correlation between the *pseudo*-constants, determined by model fitting, with their respective radiant power value for each wavelength experiment, yielded straight lines (r^2 > 0.96) with intercepts close to zero (Table 3), as predicted by Eqs.4 and 6a. Incidentally, these results also support the validity of the proposed model equations (Eqs.(3)–(6)).

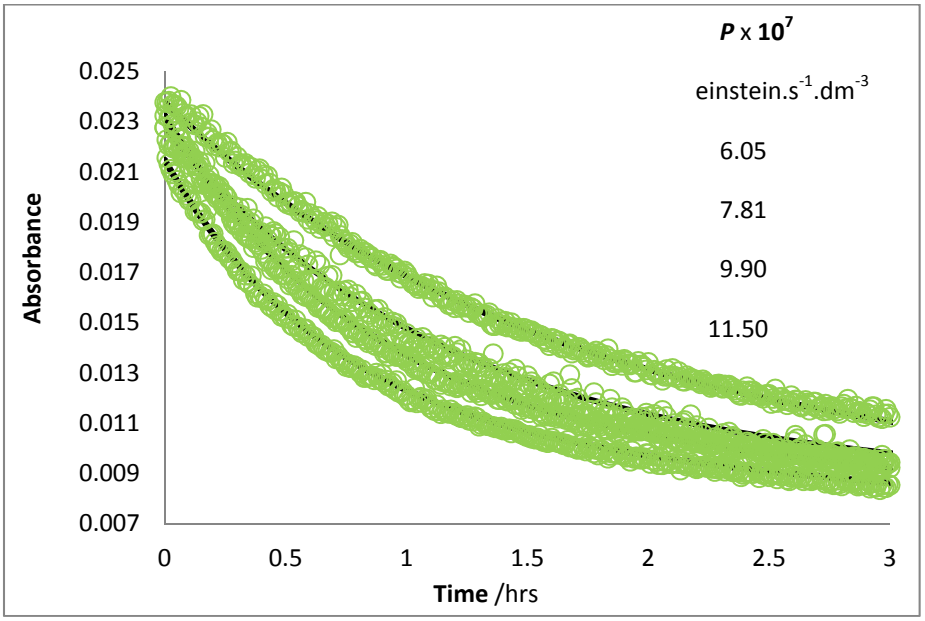

Figure 11. Effect of increasing the irradiation radiant power ($P_{\lambda_{irr}}$) on the kinetic traces of Ribo (1.50 x 10^{-6} M) when irradiated and observed at 445 nm. The circles represent the experimental data while the lines represent Eq.5 fittings.

The $\beta_{\lambda_{irr}}$ and $\delta_{\lambda_{irr}}$ factors are independent of the intensity of radiation and can thus offer an advantage in allowing effective comparisons of photoreactions rates to be made between

the same set of studies or between different studies and even for different molecules. This is due to the radiant power being hardly replicable between different irradiation experiments and laboratories, and as a result the overall rate-constant could not be suitable for such comparisons. For instance, these factors could be used to establish a photoreactivity scale whereby drugs are ranked according to their e.g. $\beta_{\lambda_{irr}}$value. We propose here a provisional scale as given in Table 4. For experiments where the concentrations and/or irradiation path-lengths (e.g. Exp_1 and Exp_2) are different, their corresponding $\beta_{Exp_1}^{\lambda_{irr}}$ and $\beta_{Exp_2}^{\lambda_{irr}}$ can be adjusted to account for the variation in concentration and/or irradiation path-length in order to compare the photoreactions rates of the molecule(s).

Table 3: Correlation between $k_{A\rightarrow B_1}^{\lambda_{irr}}$, $k_{B_1\rightarrow B_2}^{\lambda_{irr}}$, and υ_o with radiant power ($P_{\lambda_{irr}}$), for Ribo (1.8 x 10^{-6} M) photodegradation in ethanol ($l_{\lambda_{irr}}$= 2 cm; $l_{\lambda_{obs}}$= 1 cm) together with the corresponding $\beta_{\lambda_{irr}}$ or $\delta_{\lambda_{irr}}$ and the span of radiant power employed for various monochromatic irradiations.

$\boldsymbol{\lambda_{irr}}$ / nm	**Equation of the line** [a,b]			$\boldsymbol{P_{\lambda_{irr}} \times 10^7}$ /einst.s^{-1}.dm^{-3}
	$\boldsymbol{k_{A\rightarrow B_1}^{\lambda_{irr}} = \beta_{A\rightarrow B_1}^{\lambda_{irr}} \times P_{\lambda_{irr}}}$	$\boldsymbol{k_{B_1\rightarrow B_2}^{\lambda_{irr}} = \beta_{B_1\rightarrow B_2}^{\lambda_{irr}} \times P_{\lambda_{irr}}}$	$\boldsymbol{\upsilon_o = \delta_{\lambda_{irr}} \times P_{\lambda_{irr}} + intercept}$	
420	$302.22\times P_{420} - 3\times 10^{-5}$	$3.52\times P_{420} - 5\times 10^{-7}$	$-2.88\times P_{420} + 6\times 10^{-7}$	6.27 – 1.30
445	$421.9\times P_{445} - 5\times 10^{-5}$	$43.7\times P_{445} - 3\times 10^{-5}$	$-4.15\times P_{445} - 3\times 10^{-7}$	6.05 – 12.5
460	$305.1\times P_{460} + 8\times 10^{-5}$	$41.9\times P_{460} - 2\times 10^{-5}$	$-2.49\times P_{460} - 1\times 10^{-6}$	7.46 – 1.39
480	$225.8\times P_{480} + 4\times 10^{-5}$	$39.7\times P_{480} - 2\times 10^{-5}$	$-7.21\times P_{480} + 5\times 10^{-6}$	8.17 – 19.2

a: $k^{\lambda_{irr}}$ and intercepts expressed in s^{-1}; $\beta_{\lambda_{irr}}$ in $einstein^{-1}$ dm^3. b: squared correlation coefficient ranging between 0.99 and 0.96.

518 The adjustment is achieved by dividing $\beta_{Exp_2}^{\lambda_{irr}}$ by the ratio $(F_{Exp_2}^{\lambda_{irr}} \times l_{Exp_2}^{\lambda_{irr}})/(F_{Exp_1}^{\lambda_{irr}} \times l_{Exp_1}^{\lambda_{irr}})$

519 and comparing it to $\beta_{Exp_1}^{\lambda_{irr}}$ or dividing $\beta_{Exp_1}^{\lambda_{irr}}$ by the ratio $(F_{Exp_1}^{\lambda_{irr}} \times l_{Exp_1}^{\lambda_{irr}})/(F_{Exp_2}^{\lambda_{irr}} \times l_{Exp_2}^{\lambda_{irr}})$ and

520 comparing it to $\beta_{Exp_2}^{\lambda_{irr}}$.

521

522 This approach might allow (i) a universal standardisation of photokinetic studies irrespective
523 of the light source used, provided that the study is conducted using monochromatic beams;
524 (ii) a standard and quantitative kinetic data treatment method of photodegradation results
525 and (iii) a provision for drugs' photostability scale.

526 **Table 4**: Comparative $\beta_{\lambda_{irr}}$ values for several drugs and a proposal for a ranking scale.

Drug	*Pseudo*-rate constant	Ranking Group
Montelukast	2251 – 28069	**Group I** : $\beta > 10^4$
Axitinib	2193 – 14552	
Nisoldipine	7558 – 8851	**Group II** : $6 > \beta \times 10^{-3} > 10$
Sunitinib	1560 – 5847	
Dacarbazine	2121 – 4013	**Group III** : $2 > \beta \times 10^{-3} > 6$
Fluovoxamine	818 – 2077	
Riboflavine	226 – 422	**Group IV** : $\beta < 2000$
FMF	4 – 44	

3.5. Ribo actinometry

An additional benefit procured by the $\beta_{\lambda_{irr}}$ factors is the development of new actinometric systems. In the case of Ribo, the linear correlation between its overall rate-constant of photodegradation with radiant power (Table 3) highlights its utility as an actinometric tool in the 400-480 nm spectral range. In addition, the fact that $\beta_{\lambda_{irr}}$ factors present triangular correlations with λ_{irr} (Fig.12), as has previously been observed for Sunitinib,[37] allows the determination of values of these factors at any wavelength between 420 and 480 nm (using the given equations laid out in Fig.12).

Therefore, the determination of the radiant power intensity of a monochromatic beam (in the range 420 – 480 nm) of unknown intensity can be achieved by preparing an ethanolic

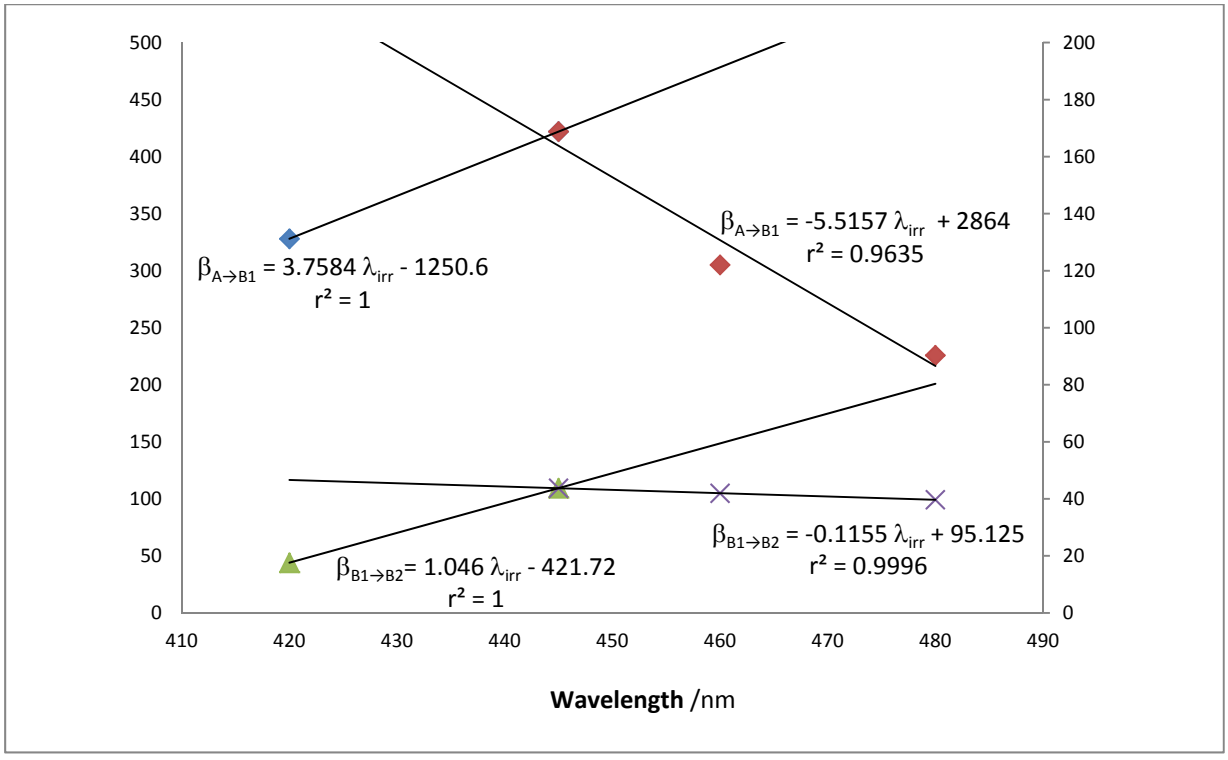

Figure 12: Variation of the pseudo-rate-constant with irradiation wavelength for each photoreaction step Ribo (1.8×10^{-6} M) photodegradation in ethanol ($l_{\lambda_{irr}}$= 2 cm; $l_{\lambda_{obs}}$= 1 cm).

542 solution of 1.8 x 10^{-6} M and irradiating it with the irradiation source of interest. The overall
543 rate-constants of the solution photodegradation kinetics can then be determined by fitting
544 it to Eq.(5). The determined $k_{A\rightarrow B_1}^{\lambda_{irr}}$ or $k_{B_1\rightarrow B_2}^{\lambda_{irr}}$ together with the corresponding $\beta_{A\rightarrow B_1}^{\lambda_{irr}}$ or
545 $\beta_{B_1\rightarrow B_2}^{\lambda_{irr}}$, respectively can then be substituted into Eq.9 (which has been derived from Eq.4),
546 to determine the unknown, $P_{\lambda_{irr}}$. A similar approach can be adopted for ${\upsilon_o}^{\lambda_{irr}/\lambda_{obs}}$ and
547 $\delta_{\lambda_{irr}}$.

548

$$P_{\lambda_{irr}} = \frac{k_{A\rightarrow B_1}^{\lambda_{irr}}}{\beta_{A\rightarrow B_1}^{\lambda_{irr}}} = \frac{k_{B_1\rightarrow B_2}^{\lambda_{irr}}}{\beta_{B_1\rightarrow B_2}^{\lambda_{irr}}} = \frac{{\upsilon_o}^{\lambda_{irr}/\lambda_{obs}}}{\delta_{\lambda_{irr}}} \quad (9)$$

549

550 This methodology now offers a series of reliable actinometers that cover the UV and Visible
551 (260 – 570 nm) dynamic range including Fluvoxamine (260 – 290 nm),[29] Dacarbazine (270 –
552 350 nm),[36] Montelukast (260 – 380 nm),[35] Axitinib (290 – 380 nm),[39] Nifedipine (280 – 400 nm),[12]
553 Nisoldipine (320 – 400 nm),[38] Sunitinib (320 – 480 nm),[37] Riboflavin (420 – 480 nm), and Diethylarene
554 (405 – 570 nm).[10] They also provide a wide range of photoreactivities as some are suitable for
555 relatively fast reactions ($\beta > 10^4$) and others to relatively slow ones ($\beta < 500$).

556

557

558

559

560

4. Conclusion

The methodology adopted here has proven to be a very useful tool to developing semi-empirical integrated rate-laws for photoreactions. It has successfully been used to elaborated a system of equations that faithfully describe $AB_4(4\Phi)$ photokinetics. These findings provide better tools for photodegradation studies than the classical approach.

The photodegradation reaction of Ribo in ethanol was well described by the $AB_2(2\Phi)$ kinetic model. The determination of all the unknowns of the photoreaction was performed by a new elucidation method. The quantum yields of Ribo and its photodegradation product FMF were found to be wavelength-dependent, increasing with wavelength in the visible region of the spectrum, and well quantified by sigmoid functions. A trend that might characterise drugs in general as it has been recurrently observed for a few active ingredients. The model equations have also allowed the establishment of Ribo as an actinometer for the irradiation range 400 - 480 nm.

The analysis of *pseudo*-rate-constants ($\beta_{\lambda_{irr}}$) could bring a simple way of categorising the photodegradation of drugs. We have proposed a scale combining four groups, from highly photoreactive to moderate and low photoreactive species, according to their $\beta_{\lambda_{irr}}$ values.

The Φ-order kinetics open for the first time new horizons for rationalisation and harmonisation of photoreactions kinetics. It might contribute to amend the procedures of the ICH recommendation on photostability testing.

582 References

583 **1.** Turro NJ, Ramamurthy V, Scaiano JC. 2009. Principles of molecular photochemistry: An
584 introduction. California: University Science Books.
585 **2.** Piechocki JT, Thoma K. 2010. Pharmaceutical Photostability and Photostabilisation
586 Technology. London: Informa Healthcare.
587 **3.** Gorner H. 2010. Photocyclization of 2,6-dichlorodiphenylamines in solution. J
588 Photochem Photobiol A: Chem 211:1–6.
589 **4.** Wu Y, Kookana R. 2011. Aqueous Photodegradation of Selected Antibiotics under
590 Different Conditions. *2010 International Conference on Biology, Environment and*
591 *Chemistry, IPCBEE vol.1, IACSIT Press, Singapore, 191-194.*
592 **5.** Fasani E, Albini A, Mella M. 2008. Photochemistry of Hantzsch 1,4-dihydropyridines and
593 pyridines. Tetrahedron 64:3190–3196.
594 **6.** Gilbert A, Bagott J. 1991. Essentials of molecular photochemistry. Oxford: Blackwell
595 Science.
596 **7.** Tonnesen HH. 2004 Photostability of drugs and drug formulations (second Ed.). London:
597 CRC Press.
598 **8.** Albini A, Fasani E. 1998. Drugs Photochemistry and Photostability. Cambridge :The
599 Royal Society of Chemistry.
600 **9.** Maafi M, Brown RG. 2007. The kinetic model for AB(1Φ) systems. A Closed-form
601 integration of the differential equation with a variable photokinetic factor. J Photochem
602 Photobiol A: Chem 187:319–324.
603 **10.** Maafi M. 2010. The potential of AB(1Φ) systems for direct actinometry. Diarylethenes
604 as successful actimometers for the visible range. Phys Chem Chem Phys 12:13248–
605 13254.
606 **11.** Maafi M, Brown RG. 2008. Kinetic analysis and elucidation options for AB(1k,2Φ)
607 systems: new spectrokinetic methods for photochromes. Photochem Photobiol Sci
608 7:1360–1372.
609 **12.** Maafi W, Maafi M. 2013. Modelling Nifedipine Photodegradation, Photostability and
610 Actinometric Properties. Int J Pharm 456:153–164.
611 **13.** Maafi M, Maafi W. 2014. Φ-order kinetics of photoreversible drug reactions. Int J Pharm
612 471:536–543.
613 **14.** De Souza ACS, Ferreira CV, Juca MB. 2005. Riboflavin : A multifuctional vitamin. Quimica
614 Nova 28:887–891.
615 **15.** Powers HJ. 2003. Riboflavin (vitamin B_2) and health. Am J Clin Nutr 77:1352–1360.
616 **16.** Ashoori M, Saedisomeolia A. 2014. Human and Clinical Nutrition Riboflavin (vitamin B_2)
617 and oxidative stress: a review. Brit J Nutr 111:1985–1991.
618 **17.** Dewick PM. 1998. Medicinal natural products. Chichester: John Wiley & Sons.
619 **18.** Ahmed I, Fassihullah Q, Noor A, Ansari IA, Ali QNM. 2004. Photolysis of riboflavin in
620 aqueous solution: a kinetic study. Int J Pharm 280:199–208.
621 **19.** Schramm M, Wiegmann K, Schramm S, Gluschko A, Herb M, Utermöhlen O, Krönke M.
622 2014. Riboflavin (vitamin B_2) deficiency impairs NADPH oxidase 2 (NOx2) priming and
623 defence against *Listeria monocytogenes*. Eur J Immunol 44:728–741.
624 **20.** Corbin F., 2002. Pathogen inactivation of blood components: Current status and
625 introduction of an approach using riboflavin as a photosensitizer. Int J hemat 76, 253–
626 257.

21. Sheraz MA, Kazi SH, Ahmed S, Anwar Z, Ahmed I. 2014. Photo, thermal and chemical degradation of riboflavin. Beilstein J Org Chem 10:1999–2012.

22. Koziol J. 1966. Studies on flavins in organic solvents-II. Photodecomposition of riboflavin in the presence of oxygen. Photochem Photobiol 5:55–62.

23. Ahmad I, Sheraz MA, Ahmed S, Kazi SH, Mirza T, Aminuddin M. 2011. Stabilizing effect of citrate buffer on the photolysis of riboflavin in aqueous solution. Results in Pharma Sci 1:11–15.

24. Ahmad I, Ahmed S, Sheraz MA, Vaid FHM, Ansari IA. 2010. Effect of divalent anions on photodegradation kinetics and pathways of riboflavin in aqueous solution. Int J Pharm 390:174–182.

25. Ahmad I, Fasihullah Q, Vaid Faiyaz HM. 2006. Photolysis of formylmethylflavin in aqueous and organic solvents. Photochem Photobiol Sci 5:680–685.

26. Ahmad I, Fasihullah Q, Vaid Faiyaz HM. 2006. Effect of light intensity and wavelengths on photodegradation reactions of riboflavin in aqueous solution. J Photochem Photobiol B: Biol 82:21–27.

27. Moore WM, Ireton RC. 1977. The photochemistry of riboflavin-V. The photodegradation of isoalloxazines in alcoholic solvents. Photochem Photobiol 25:347–356.

28. Koziol J. 1966. Studies on flavins in organic solvents-I. Spectral characteristics of riboflavin, riboflavin tetrabutyrate and lumichrome. Photochem Photobiol 5:41–54.

29. Maafi M, Lee LY. 2015. Actinometric and Φ-order photodegradation properties of anti-cancer Sunitinib. J Pharm Biomed Ana 110:34–41.

30. Heelis PF. 1982. The photophysical and photochemical properties of flavins (isoalloxazines). Chem Soc Rev 11:15–39.

31. Chacon JN, McLearie J, Sinclair RS. 1988. Singlet oxygen yields and radical contributions in the dye-sensitised photo-oxidation in methanol of esters of polyunsaturated fatty acids (oleic, linoleic, linolenic and arachidonic). Photochem Photobiol 47:647–656.

32. Grodowski MS, Veyret B, Weiss K. 1977. Photochemistry of flavins. II. Photophysical properties of alloxazines and isoalloxazines. Photochem Photobiol 26:341–352.

33. Sikorska E, Khmelinskii E, Komasa A, Koput J, Ferreira LFV, Herance JR, Bourdelande JL, Williams SL, Worrall DR, Insinska-Rak M, Sikorski M. 2005. Spectroscopy and photophysics of flavin related compounds: Riboflavin and iso-(6,7)-riboflavin. Chem Phys 314:239–247.

34. Insinska-Rak M, Golczak A, Sikorski M. 2012. Photochemistry of Riboflavin derivatives in methanolic solutions. J Phys Chem A 116:1199–1207.

35. Maafi M, Maafi W. 2014. Montelukast photodegradation: Elucidation of Φ-order kinetics, determination of quantum yields and application to actinometry. Int J Pharm 471:544–552.

36. Maafi M, Lee LY. 2015. Determination of Dacarbazine Φ-order photokinetics, quantum yields, and potential for actinometry. J Pharm Sci 104:3501–3509.

37. Maafi M, Lee LY. 2015. Actinometric and Φ-order photodegradation properties of anti-cancer Sunitinib. J Pharm Biomed Ana 110:34–41.

38. Maafi M, Maafi W. 2015. Quantification of Unimolecular Photoreaction Kinetics: Determination of Quantum Yields and Development of Actinometers—The Photodegradation Case of Cardiovascular Drug Nisoldipine. Int J Photoenergy 1–12.

39. Unpublished data.

40. Moore WM, Baylor C-Jr. 1969. The photochemistry of riboflavin. IV. The photobleaching of some nitrogen-9 substituted isoalloxazines and flavins. J Amer Chem Soc 91: 7170.

41. Holzer W, ,Shirdel J, Zirak P, Penzkofer A, Hegemann P, Deutzmann R, Hochmuth E. 2005. Photo-induced degradation of some flavins in aqueous solution. Chem Phys 308:69-78.

42. Insińska-Rak M, Golczak A, Sikorski M. 2012. Photochemistry of riboflavin derivatives in methanolic solutions. J Phys Chem A 116:1199-207.

43. Insińska-Rak M, Sikorska E, Bourdelande JL, Khmelinski IV, Prukala W, Dobek K, Karolczak J, Machado IF, Ferreira LFV, Dulewicz E, Komasa A, Worrall DR, Kubicki M, Sikorski M. 2007. New photochemically stable riboflavin analogue : 3-Methyl-riboflavin tetraacetate. J Photochem Photobiol A: Chem 186:14-23.

44. The Photoisomerization of azobenzene. G. Zimmerman, L-Y Chow, U-J Paik. J. Am. Chem. Soc., 1958,80(14), pp 3528–3531.

45. Montalti M, Credi A, Prodi L, Gandolfi MT. 2006. Handbook of photochemistry. 3rd Ed. Boca Raton. CRC Press Taylor & Francis.

46. Mohammed OF, Vauthey E. 2008. Excited-state dynamics of nitroperylene in solution: solvent and excitation wavelength dependence. J Phys Chem A 112:3823-3830

47. Mazzoni M, Agati G, Troup GJ, Pratesi R. 2003. Analysis of wavelength-dependent photoisomarization quantum yield in bilirubins by fitting two exciton absorption bands. J Opt A: Pure appl. Opt. 5:S374-S380.

48. Hansom KM, Simon JD. 1998. The origin of the wavelength-dependent photoreactivity of trans-urocanic acid. Photochem Photobiol 67:538-540.

49. The effect of wavelength on organic photoreactions in solution. Reactions from upper excited state. Turro NJ, Ramamurthy V, Cherry W, Farneth W. 1978. Chem Rev 78:125-145.